NASA Technical Memorandum 83520

NASA-TM-83520 19840012252

Low Frequency Noise in a Quiet, Clean, General Aviation Turbofan Engine

Ronald G. Huff, Donald E. Groesbeck,
and Jack H. Goodykoontz
Lewis Research Center
Cleveland, Ohio

January 1984

NASA

51 1 1 RN/NASA-TM-83520

DISPLAY 51/2/1

84N20320*# ISSUE 10 PAGE 1575 CATEGORY 71 RPT#: NASA-TM-83520
E-1879 NAS 1.15:83520 84/01/00 55 PAGES UNCLASSIFIED DOCUMENT

UTTL: Low frequency noise in a quiet, clean, general aviation turbofan engine

AUTH: A/HUFF, R. G.; B/GROESBECK, D. E.; C/GOODYKOONTZ, J. H.

CORP: National Aeronautics and Space Administration. Lewis Research Center, Cleveland, Ohio. AVAIL.NTIS SAP: HC A04/MF A01

MAJS: /*EXHAUST NOZZLES/*JET AIRCRAFT NOISE/*NOZZLE FLOW/*TURBOFAN ENGINES

MINS: / AEROTHERMODYNAMICS/ DATA BASES/ FLOW VELOCITY/ PREDICTION ANALYSIS TECHNIQUES/ PRESSURE DISTRIBUTION

ABA: Author

ABS: A quiet, clean, general aviation, turbofan engine was instrumented to measure the fluctuating pressures in the combustor, turbine exit duct, engine nozzle and the far field. Both a separate flow nozzle and an internal mixer nozzle were tested. The fluctuating pressure data are presented in overall pressure and power levels and in spectral plots. The combustor data are compared to recent theory and found to be in excellent agreement. The results indicate that microphone correction procedures for elevated mean pressures are questionable. Ordinary coherence function analysis suggests the presence of an additional low frequency noise source downstream of the turbine that is due to the turbine itself. Low frequency narrowband data and coherence function analysis are presented.

ENTER:

LOW FREQUENCY NOISE IN A QUIET, CLEAN, GENERAL AVIATION TURBOFAN ENGINE

Ronald G. Huff, Donald E. Groesbeck and Jack H. Goodykoontz

National Aeronautics and Space Administration
Lewis Research Center
Cleveland, Ohio 44135

SUMMARY

A quiet, clean, general aviation, turbofan engine has been instrumented to measure the fluctuating pressures in the combustor, turbine exit duct, engine nozzle and the far field. Both a separate flow nozzle and an internal mixer nozzle were tested. The fluctuating pressure data are presented in overall pressure and power levels and in spectral plots. The combustor data are compared to recent theory and found to be in excellent agreement. The results indicate that microphone correction procedures for elevated mean pressures may be questionable. Ordinary coherence function analysis suggests the presence of an additional low frequency noise source downstream of the turbine that may be due to the turbine itself. Low frequency narrowband data and coherence function analysis are presented.

E-1879

INTRODUCTION

Noise generated inside aircraft turbine engines has been shown to be a potential problem at reduced power settings (refs. 1 to 13). The exact source of this noise has not been clearly defined. In recent years measurements of fluctuating pressures in aircraft type turbine engine combustors and tailpipes have been made in both engines and component test rigs (refs. 2 to 11 and 13 to 24). Internal engine measurements have generally been made in conjunction with far field acoustic measurements (refs. 2 and 3, and 5 to 11). As part of an overall experimental program established to produce a core engine noise data base, the Airesearch quiet, clean, general aviation turbofan engine (QCGAT, ref. 26) was instrumented to measure internal fluctuating pressures and far field noise.

Empirical correlations have been generated, using the existing data base, to predict the low frequency noise generated by turbine engines. More recently a theoretical analysis of the pressure fluctuations generated in the combustor has been reported (ref. 25). The theory requires that a constant associated with the type of combustor and the combustor configuration be determined from the data base, for use when predicting the fluctuating pressure spectrum and the overall sound pressure level.

The present work has a two-fold objective: (1) to enlarge the present data base on core engine noise covering a range of engine configuration and size; and (2) to test the theory of reference 25 to determine its ability to predict the fluctuating pressure levels in combustors using the constants determined from the previously obtained data base. Two nozzle configurations were tested. Data is presented herein for both the separate flow and the mixer nozzle configurations. Internal and far field spectra are presented. The low frequency (below 2000 Hz) overall acoustic power level is presented as

a function of the effective jet exhaust velocity and combustor heat release rate. The measured, low frequency, combustor sound pressure level is compared to the theory of reference 25. Both one-third octave and narrowband spectra are presented.

The ordinary coherence functions have been obtained for the two configurations at two representative engine speeds and are presented herein for the following sets of sensors:

(1) Combustor-turbine
(2) Combustor-nozzle exit
(3) Combustor-far field
(4) Turbine-core nozzle exit
(5) Turbine-far field
(6) Core nozzle exit-far field

SYMBOLS

A area, m^2

C sonic velocity, m/s

Δf band width, Hz

I acoustic intensity, W/m^2

M Mach number

N the exponent of 2 indicating the number of averages in coherence analysis, that is 2^N = number of samples used in average.

$\overline{P}$ acoustic power, W

p rms acoustic or fluctuating pressure, N/m^2

Q heat release rate, W

V_c velocity at the core engine nozzle exit, m/s

V_e effective jet velocity at exit of separate flow nozzle engine configuration, m/s

V_f velocity of flow at fan nozzle exit, m/s

W_c core engine mass flow rate, kg/s

W_f fan mass flow rate, kg/s

ρ mean static density of gas, kg/m^3

γ ordinary coherence function

$\Delta\tau$ cross correlation time increment, s

TEST ENGINE DESCRIPTION

The Airsearch QCGAT turbofan engine with reverse flow combustor was designed to have 1767 kg (3892 lb) thrust with ground test nacelle, acoustic treatment and mixer nozzle installed while operating at takeoff, sea-level standard day conditions. The fan to core bypass ration was 3.7 (for more details see ref. 26). The engine as installed in the vertical lift stand test facility at NASA Lewis is shown in figure 1(a). A screen is attached to the engine inlet to minimize the effect of inlet flow distortions and turbulence on the noise produced by the fan and compressor. An aft view of the engine is shown in figure 1(b). Two nozzle configurations were tested. The separate flow nozzle engine configuration pictured in figure 1(b) and shown schematically in figure 2(a) provided separate flow passages for fan and core engine flows resulting in a coaxial jet exhaust. The second nozzle configuration is called the mixer nozzle engine configuration and is pictured in figure 1(c) and shown schematically in figure 2(b). The mixer nozzle configuration consisted of a multilobed nozzle attached to the core engine just aft of the turbine exit. The fan flow was ducted around and between the lobes of the multilobed nozzle and allowed to mix with the core engine flow, in a common duct, before passing through a single convergent nozzle. The single jet exiting the engine had nonuniform temperature and velocity profiles.

Nacelle acoustic treatment consisted of absorbing liners placed in the fan inlet and exhaust ducts. The frequency range covered by the duct liners was 1600 to 5000 Hz. Details are given in reference 26.

INSTRUMENTATION

Acoustic Instrumentation

The acoustic instrumentation required for these tests may be divided into two groups, internal microphones and external far field noise (acoustic) microphones. Each group will now be discussed in appropriate detail. Preand post-run microphone calibration checks were made using a pistonphone having an output of 124 dB at 250 Hz.

Internal semi-infinite tube probes. - A detailed description of this instrumentation is given in reference 6. A summary is given here. A 0.635 cm outside diameter tube was installed with one end flush with the duct wall at the required measurement point. At an appropriate distance from the duct wall external to the engine a tee is placed in the line and a 0.635 cm microphone enclosed in a pressure vessel is inserted in the side leg of the tee. Attached to the remaining leg at the tee is a length of tubing of sufficient length to minimize reflections from its end. Nitrogen purge gas is forced into the end of the tubing and regulated to a pressure just above the static pressure in the engine duct. This creates a positive flow of nitrogen into the duct and prevents the hot engine gases from reaching the tee and microphone location. The pressure in the vessel containing the microphone is regulated to just above engine duct pressure. Thus, as the engine speed varies the microphone environmental pressure will vary. Since the microphone output is sensitive to pressure the vessel pressure was recorded and the microphone output corrected mathematically during the data conduction process (except for the narrowband

spectral analysis). The correction, supplied by the manufacturer, ranged from zero at atmospheric pressure to plus 4.2 dB at 100-percent engine operating speed for the combustor microphone (12 atm).

The internal fluctuating pressures were measured in the following components as shown in figure 2: (1) combustor, (2) turbine exit duct, (3) core nozzle exit (fig. 2(a)) or mixer nozzle exit (fig. 2(b)).

External far field microphones. - The far field acoustic measurements were made using 1.27 cm condenser microphones arranged around a semicircle beginning at 40° off the engine inlet axis and extending through 160° (fig. 3). The center of the circle was at the core nozzle exit or mixed flow common nozzle exit. The microphones were placed on the ground pointed at the center of the circle at a constant radius of 24.4 meters.

Engine Operating Instrumentation

For these acoustic tests the engine had a minimum of internal pressure and temperature sensors. In order to convert the fluctuating pressures to an acoustic intensity it is necessary to know the static pressure and temperature at each measurement point in the engine. Because of the lack of instrumentation at the measuring points, and because the acoustic information does not require extreme accuracy in mean values of pressure and temperatures, the required aerothermodynamic information was determined from the engine performance computer program provided by the manufacturer. Engine speed was recorded along with atmospheric temperature and pressure. As discussed in the internal semi-infinite tube probe section of this report the microphone ambient pressure was controlled to approximately the engine static pressure. This pressure was recorded for use in correcting the microphone measured values for decreased sensitivity as directed by the microphone manufacturer.

DATA RECORDING AND PROCEDURE

The internal and far field microphone outputs were recorded simultaneously on high density tape with FM tape recorders. A 2-minute recording time was used. The engine fan, low and high pressure turbine speeds; atmospheric temperature and pressure and microphone vessel pressures were recorded using the automatic data acquisition system. Three sets of engine operation data were recorded during the taping of the acoustic data.

The precedure followed in acquiring the data was designed to minimize the effect of external noise sources on the data. The engine was first brought to a stable, required operating speed. When it was assured that two minutes of low background noise was available, the tape recorders were started and a minimum of two minutes of fluctuating pressure data were recorded. This procedure was repeated until the range of operating speeds was completed. The microphones were calibrated using the pistonphone before and after the test to insure that they were in operating tolerance during the test.

DATA REDUCTION

The reduction of data to the desired usable quantities may be divided into three parts. These are: engine aerothermodynamic data, acoustic spectral analysis, and acoustic power computations. A discussion of each part follows.

Engine Aerothermodynamic Data

The manufacture's engine performance program was exercised over a range of engine corrected speeds. Engine corrected speed is the ratio of the low pressure turbine speed to the square root of the ratio of ambient temperature to standard day temperature (288 K). For each of the two engine nozzle configurations the mass flow rates, pressures and temperatures were calculated as a function of low pressure turbine speed and probe location. A curve fit was produced for mass flow rate, pressure and temperature at each probe station as a function of low pressure turbine corrected speed. Engine speeds recorded for each test point were averaged and the average value was used in conjunction with the above curve fits to obtain the mass flow rate, pressure and temperature at each of the internal fluctuating pressure microphone probe locations. Corrected weight flow was used to calculate the Mach number at the probe location. The sonic velocity, C, and gas density, ρ, were calculated assuming adiabatic expansion of a perfect gas.

An effective jet velocity for the separate flow nozzle is given in reference 13. The equation for the effective velocity, V_e, is:

$$V_e = \frac{\frac{W_f}{W_c} V_f + V_c}{\frac{W_f}{W_c} + 1} \qquad (1)$$

The quantities required in the above equation were obtained from the engine performance program and curve fitted in the same manner as the pressures and temperatures described in this section.

The effective velocity for the mixer nozzle is the mixer nozzle average exhaust velocity determined using the above described curve fit procedure.

Acoustic Spectral Analysis

The fluctuating pressure signals from selected tape recorder channels were analyzed after the engine tests were completed (off line). Both one-third octave and narrowband analyses were performed using a fast Fourier transform (FFT) analyzer. The data were transmitted to a large main frame computer, compensated for amplifier gain settings used while recording and stored. The narrowband data (frequency range 0 to 2000 Hz) were plotted as out-put by the computer on a machine plotter. The one-third octave data 25 to 2000 Hz were used to compute the overall sound pressure level using a reference pressure 2×10^{-5} Pa. The fluctuating pressure microphone data were corrected for environmental pressure as discussed under the instrumentation section. The

correction ranged from 1 dB to 4.2 dB at the 40 and 100 percent speed points respectively. The narrowband data have not been corrected in this manner and appear in this report as analyzed by the FFT analyzer.

Acoustic Power Computation

The acoustic power calculated for the one-third octave pressure spectrum measured inside the engine by the fluctuating pressure microphones is calculated assuming that a plane wave exists in the duct without reflections. This is a gross oversimplification of the acoustic field in the duct but is used herein to calculate the power for lack of a better method. The intensity is:

$$I = \frac{p^2}{\rho C}(1 + M) \tag{2}$$

The plane wave power is related to intensity by:

$$\overline{P} = IA \tag{3}$$

where: A is the cross sectional area of the duct at the measuring station and intensity I is given above (eq. (2)).

The power levels given herein are referenced to 10^{-13} watt. Overall levels were determined by summing the acoustic pressure squared over the frequency range of interest, usually 25 to 2000 Hz.

RESULTS AND DISCUSSION

The engine was operated over a range of low pressure turbine corrected speeds from 40 to 100 percent of maximum speed. The data presented are those measured by the internal microphones in the engine at the combustor, turbine exit, and nozzle exit and by the far field microphone located 120° from the engine inlet axis and 24.4 meter radial distance from the engine exit plane. This far field location was selected because it yields the peak sound pressure level for low frequency core noise.

In the following discussion the spectral and overall pressure and power levels will be presented. Representative narrowband spectra will be discussed and comparisons of the ordinary coherence function will be made for various combinations of sensors. Additional narrowband pressure spectra and coherence functions are presented in Appendixes A and B, respectively.

Sound Pressure Level

The one-third octave spectra presented herein have been corrected for the microphone environmental pressure as described in the instrumentation section of this report.

Separate flow nozzle spectra. - The one-third octave band pressure spectra covering the 25 to 20 000 Hz frequency range are presented in figure 4 for the

separate flow nozzle configuration. The pressure level downstream of the turbine is less than that in the combustor by approximately 10 dB at both the 40 and 89 percent engine speeds (figs. 4(a) and 4(b)) and their spectral shapes are similar. For both speeds the pressure at the nozzle exit is less than at the turbine exit station. The trend is to lower pressure levels in moving from the combustor through the turbine and core nozzle to the far field. For the 40 percent speed (fig. 4(a)) the shape of the nozzle pressure spectrum is similar to the far field spectrum.

Mixer nozzle spectra. - The pressure level for the mixer nozzle configuration (fig. 5) also decreases from the combustor through the engine to the far field microphone. However, the spectral shape at the turbine exit station is considerably different than the combustor spectrum. A pronounced hump centered at 200 Hz occurred in the turbine exit spectrum. At 40 percent speed (fig. 5(a)) the turbine exit and nozzle exit spectra are more similar in shape than the combustor and turbine exit. At 89 percent speed (fig. 5(b)) the turbine exit and nozzle exit spectral shapes at high frequencies (greater than 800 Hz) are close; but at the 40 percent speed (fig. 5(a)) they come together at frequencies greater than 6300 Hz where turbine tones control the spectra. A similar result was observed at 40 percent speed for the separate flow nozzle (fig. 4(a)). The spectral shape and magnitude might be expected to agree between the turbine exit and nozzle exit stations because they both "see" the internal mixing noise source. For both the 40 and 89 percent speeds the nozzle exit and far field spectra have similar spectral shapes.

Far field broadband spectra. - The one-third octave spectra, to 20 000 Hz, for the far field microphone station are presented in figures 6(a) and 6(b) for the separate flow and mixer nozzle configurations respectively over the range of engine speeds. The spectra increase in level with engine speed as might be expected. Comparison of the separate flow nozzle spectrum (fig. 6(a)) with the mixer nozzle spectrum (fig. 6(b)) shows that both have low frequency peaks, but that the mixer nozzle spectrum exhibits more prominent peaks around frequencies of 160 to 200 Hz. This may be the result of the geometric differences between the separate flow and mixer nozzles that result in different core nozzle acoustic transmission and/or jet mixing properties and profiles.

Low-frequency internal pressure spectra. - The one-third octave pressure spectra from 25 to 2000 Hz are presented in figure 7 for both the separate flow and the mixer nozzle configurations over a range of engine test speeds. As expected the combustor spectra from the separate flow nozzle test (fig. 7(a)) and the mixer nozzle test (fig. 7(b)) are essentially the same. No deviation is expected because the configuration changes were all made downstream of the turbine. However, the 40 percent speed spectra obtained during the separate flow test is considerably different from any other spectrum for either nozzle. No explanation for this is available at this writing. It may be that some critical operating condition exists concerning impending instabilities but his cannot be confirmed and is only postulated at this time.

The low frequency pressure spectra measured in the two tailpipe ducts (fig. 2) are shown in figure 8 over a range of operating speeds. The spectra of the separate flow configuration are shown in figure 8(a). The low frequency spectra peak at 315 Hz. Similar spectra are presented in figure 8(b) for the mixer nozzle configuration. These spectra do not exhibit a consistent well defined peak.

Combustor Overall Pressure Level - Theory Comparison

As discussed previously one of the objectives of this test was to provide fluctuating pressure data from a combustor for comparison with a theoretical prediction (ref. 25). The measured combustor overall pressure level, not corrected for microphone environmental pressure, is shown in figure 9(a) as a function of engine speed. The theory of reference 25 is represented by the solid line with the same value for the constant as described in reference 25. Almost perfect agreement between the theory and the as-measured pressure level has been obtained. If, however, the fluctuating pressure data is corrected for environmental pressure as described previously, the overall pressure level deviates from the theory as shown in figure 9(b). In reference 25 the theory was compared with measured data obtained using standard pressure sensors that do not require correction for static pressure level. The data and theory agree extremely well over the entire range of engine thrust from 3.8 to 100 percent of maximum. This is also true of the present data if the environmental pressure correction is not applied. This finding calls into question the method of correcting microphone type fluctuating pressure measurements for environmental pressure effects.

Power Level

The power level associated with the fluctuating pressures presented in this report has been calculated assuming that the pressure waves are acoustic plane waves and that there are no reflections. This approach is completely justified for the far field microphones. Measurements of fluctuating pressures in ducts with turbulent flow present the problem of sorting the turbulent from the acoustic fluctuating pressure. For purposes of this report the usual assumption has been made, that is, the pressure fluctuations are acoustic. Equations (2) and (3) were used to calculate the acoustic power in the duct. The acoustic power in the far field is calcuated using these equations and setting the Mach number to zero. The acoustic power calculation accounts for wave front area, mean pressure and temperatures, and flow Mach number. The acoustic power level, calculated over frequencies from 25 to 2000 Hz, is presented in figure 10 as a functon of combustor heat release rate for both the separate flow and mixer nozzle configurations. Comparison of the combustor power levels between the two nozzle configurations show close agreement. The slightly different values might be the result of the slight difference in engine operating speeds, however, the variation is within the scatter of the data.

This result is to be expected because the configuration changes were made downstream of the turbine exit. The combustor acoustic power, as shown by the solid line drawn through the data in figure 10, is proportional to the combustor heat release rate to the 1.6 power. The turbine exit acoustic power for both the separate flow nozzle and the mixer nozzle (fig. 10) is substantially the same. Additionally, both configurations have far field acoustic powers that are nearly equal, except at higher power settings.

Jet noise has been shown to vary as the jet velocity to the eighth power for subsonic jets. The equivalent jet velocity has been computed using equation (1) for the separate flow nozzle configuration. The jet velocity for the mixer nozzle configuration is the mixer nozzle exit velocity calculated from

continuity. Figure 11 shows the far field and nozzle exit acoustic powers (25 to 2000 Hz) as a function of effective jet exhaust velocity for both test configurations. For purposes of estimating what part of the acoustic power generated by the engine is associated with jet noise, a line proportional to the jet velocity to the eighth power has been added. Unpublished data from a small scale jet noise test rig, has been scaled up to engine size and the overall power levels are plotted in figure 11. The data agree with the far field engine overall power levels. Small scale data are not available at the lower jet velocitites covered by the engine test. The engine data deviates from the jet noise line below the 70 percent speed point. Except for the highest velocities, within the scatter of the data, both the nozzle exit and far field acoustic power are in substantial agreement for both engine test configurations even at the lowest jet velocities.

The one-third octave power level spectra at the combustor, turbine exit, nozzle exit and far field measuring stations are presented in figures 12 and 13 for the separate flow and mixer nozzle configurations respectively. The 40 and 89 percent engine speed power spectra are given. The previously mentioned unpublished scale model spectral data from a jet noise rig operated at effective velocitites, V_e, corresponding to the 89 percent engine speed data presented herein are also shown in figures 12(b) and 13(b) for separate flow and mixer nozzles respectively. Substantial agreement between the small scale and engine far field power spectra at low frequencies, that is, less than 250 Hz, is shown. Above 250 Hz both engine configurations have higher power levels than the scaled model data. The engine mixer nozzle begins to deviate from the scale model mixer nozzle at about 100 Hz. Based on the agreement of the engine and scale model data at low frequency it is concluded that the low frequency power at the 89 percent engine speed is dominated by jet noise.

Now, comparison of the engine far field spectra to the engine nozzle exit spectra at 89 percent speed (figs. 12(b) and 13(b)) show a significant difference at the low frequencies (less than 200 Hz) that is attributed to the jet noise generated outside of the engine. At 40 percent engine speed (figs. 12(a) and 13(a)) the difference between the low frequency power level in the engine nozzle and far field is less. This result is consistent with the conclusion that the low-frequency jet noise dominates the far field as engine speed (that is jet velocity) is increased. For both nozzles the far field engine spectrum at 89 percent speed has low frequency peaks and higher frequency turbine tones that, of course, do not appear in the scale model data (fig. 13(b)).

From the above discussion the conclusion may be drawn that the mixer nozzle has little effect on the far field noise at frequencies less than 2000 Hz except at the two highest engine speeds. This may be due to domination of the far field by low frequency core noise and/or to the poor mixing of the engine flows by the mixer nozzle that gives no reduction in jet noise. Subject to the limitations resulting from the plane wave assumption the significant agreement above 200 Hz between the power levels at the nozzle exit and the far field would tend to indicate that the higher frequency noise is internally generated by the turbine at the higher frequencies and through some other internal noise sources, perhaps also the turbine, in the mid range frequencies.

Narrowband Spectra

Representative narrowband spectra are presented for each of the two nozzle configurations tests. The narrowband pressure spectra are not corrected for the microphone environmental pressure loss in sensitivity. The spectra are for the as-measured fluctuating pressures in the combustor, nozzle exit and at the 120° far field microphone location for representative speeds. Additional low frequency (less than 2000 Hz frequency) narrowband spectra are given in Appendix A for both test configurations at the combustor, turbine exit and far field 120° microphone locations.

Figure 14 presents the combustor narrowband spectra for the 40 percent speed test of both the separate flow and the mixer nozzle configurations to 10 000 Hz. In general, the spectra should be alike except for slight differences in engine speed. The levels for both configurations are approximately equal. However, the separate flow configuration (fig. 14(a)) has a tone at 3300 Hz that does not appear in the mixer nozzle configuration spectra (fig. 14(b)). Slight differences in spectral shape may be due to the interaction of acoustic waves with the combustion process. It appears that slight differences in engine operating conditions may also cause significant changes in the narrowband spectra. Figure 15 presents the 40 percent speed, narrowband spectra at the nozzle exit measuring station for both the separate flow nozzle (fig. 15(a)) and the mixer nozzle (fig. 15(b)) configurations. The frequency range is from 0 to 10 000 Hz. These spectra show tones in the range of frequencies corresponding to the blade passing frequencies of the low pressure turbine. The separate flow nozzle spectrum (fig. 15(a)) has more clearly defined pure tones than the mixer nozzle spectrum (fig. 15(b)). The "haystack" effect for the mixer nozzle may be due to the mixing of the flow in the mixer nozzle. The spectral shapes and magnitude are essentially the same except for the haystacking effect.

The 40 percent speed, far field narrowband spectra at the 120° microphone location are shown in figure 16 for both separate flow (fig. 16(a)) and mixer nozzle (fig. 16(b)) configurations. The levels are essentially the same; however, the mixer nozzle is several dB lower than the separate flow nozzle between 2000 and 5000 Hz. Comparison of the spectral shapes shows that the haystack effect is present in the far field mixer nozzle spectrum (fig. 16(b)) but is not present in the separate flow nozzle spectrum (fig. 16(a)). This effect was also observed at the nozzle exit measuring stations (fig. 15), as mentioned earlier.

At the higher engine speeds, (89 percent, fig. 17), the separate flow nozzle configuration narrowband far field spectrum shows evidence of low pressure turbine tones (fig. 17(a)). These tones are not as pronounced as they were at the lower speed (fig. 16(a)). Also comparison of the separate flow and mixer nozzle spectra (figs. 17(a) and 17(b)) shows that in the range between 5000 and 16 000 Hz the mixer nozzle sound pressure level is less than that of the separate flow nozzle by as much as 5 to 10 dB. At frequencies below 2000 Hz the spectra for both configurations are about equal. The low frequency pressure spectra (<2000 Hz) at the nozzle exit measuring station for the separate flow and mixer nozzle configurations are presented in figures 18 and 19, respectively, over a range of engine operating speeds. The separate flow nozzle spectra in general show more humps than the mixer nozzle spectra over the entire speed range given. This could be due to higher order mode cut

on as shown in reference 27. The separate flow nozzle exit spectra have peaks at frequencies of 100 and 300 Hz that appear to be independent of engine speed. The mixer nozzle spectra have a peak at 200 Hz although it is less pronounced than the peaks found in the separate flow nozzle exit spectra.

Coherence Analysis

Coherence analysis is used to determine the similarity between two signals. A cross correlation is the averaged product of the two signals obtained while introducing a time delay in one of the signals. The product so obtained is plotted as a function of the time delay. For an acoustic signal the product will reach a maximum when the time delay equals the time for the signal to travel at the speed of sound between the two measuring points. Figure 20 presents the cross correlation between the fluctuating pressure in the combustor and the acoustic pressure at the 120° far field microphone for the separate flow nozzle. An acoustic wave traveling in the atmosphere requires 72.7 ms to travel 24.4 meters. The cross correlation shows a maximum value at approximately this time delay thus indicating that the origin of the far field pressure was in the combustor and that it is acoustic in nature. In order to estimate how much of the combustor signal appears in the far field the ordinary coherence function has been computed. If the two signals are exactly alike and not contaminated by other noise the ordinary coherence will be unity. Values of the coherence function less than unity may be the result of contamination from other noise sources or the lack of similarity between the signals. Keeping this discussion in mind should aid the reader in understanding the coherence functions presented in this section. Appendix B presents detailed coherence functions for various combinations of combustor, turbine exit, nozzle exit, and far field measuring stations for both separate flow and mixer nozzle configurations operating at engine speeds of 40 to 89 percent speed.

Representative coherence functions are presented herein for comparison purposes. The bias error due to time delay was not removed from the data. The coherence function between the combustor and the 120° far field microphone is presented in figure 21 for two engine speeds for the separate flow nozzle configuration. Figure 21(a) shows a peak coherence of 0.4 at a frequency of 125 Hz, excluding the tone generated at 350 Hz, for the 40 percent engine speed. The coherence is broadbanded and is apparent out to 425 Hz. The coherence at 89 percent engine speed is shown in figure 21(b). The coherence exists to 425 Hz but its magnitude has decreased to less than 0.14. As discussed above this may be the result of contamination from other noise sources. The point is that the existence of the coherence between the combustor and the far field infers that part of the combustor noise is getting to the far field observer from the engine combustor.

The coherence function for the separate flow nozzle configuration between the turbine exit measuring station and the 120° far field microphone is presented at the 40 and 89 percent engine speeds in figures 22(a) and (b), respectively. The same trend with engine speed is apparent, that is, increasing the engine speed decreases the magnitude of the coherence function. At the low engine speed the coherence exists out to frequencies as high as 700 Hz and the coherence function has three peaks at frequencies on the order

of 125, 300, and 400 Hz; their magnitudes are 0.6, 0.62 and 0.5, respectively. At increased engine speed (fig. 22(b)) the peak coherence is only 0.2 at 300 Hz but the frequency range of measurable coherence extends to over 900 Hz.

A comparison of the coherence function for the separate flow configuration operating at 40 percent engine speed is made in figure 23 between the combustor-far field and the turbine-far field coherence functions. It appears that similar coherence functions exist between the combustor and the far field and between the turbine and far field below 200 Hz. Above 200 Hz the turbine-far field coherence function seems to be much greater than the combustor-far field. This may indicate that the turbine sees a signal that the combustor sensor cannot sense or that there is more contamination in the combustor signal. The possibility exists then, that the turbine itself generates noise in the 200 to 600 Hz range. However, no conclusive proof is available at this time. To examine the relationship between the combustor and turbine signals the coherence function between these signals has been calculated and is presented in figure 24. Coherence below a frequency of 150 Hz is on the order of 0.6. Above 150 Hz the coherence is less than 0.2 and disappears above 450 Hz. The large value of the coherence function below 150 Hz implies that the combustor and turbine signals are similar, to some degree, below this frequency. Above 150 Hz the low coherence value implies that the signals are less similar. If the turbine is choked any signal generated downstream of the turbine will not reach the combustor. In that case any noise generated by the turbine downstream of the choke point will not penetrate to the combustor sensor and the coherence function will be decreased. This could explain the lack of coherence above 150 Hz. Noise generated by the turbine would, however, be transmitted to the far field, thus accounting for the high coherence from downstream of the turbine to the far field shown in figure 23 above 200 Hz. These arguments, although circumstantial, provide a reasonable explanation for the results of the coherence functions presented herein.

To compare the separate flow nozzle with the mixer nozzle configuration the coherence functions between the separate flow core nozzle and far field and between the mixer nozzle exit and far field are presented in figure 25 for the 40 percent engine speed. The separate flow core nozzle has a much broader frequency range of coherence than the mixer nozzle. Maximum coherence for the separate flow nozzle is in excess of 0.6. For the mixer nozzle the maximum coherence function was 0.5. It is possible that more of the core noise gets to the far field from the separate flow configuration than from the mixer nozzle configuration or that mixing noise is causing a decrease in mixer nozzle to far field coherence. A comparison is made in figure 26 at the 40 percent engine operating speed of the coherence function between the combustor and core nozzle exit for the separate flow nozzle and between the combustor and mixer nozzle exit pressure signals. The separate flow nozzle has greater coherence below 125 and above 175 Hz than the mixer nozzle configuration. This might be expected since the mixer nozzle internal mixing noise may act as a third noise source tending to decrease the coherence function. However, the general shape of both coherence functions are similar. This is to be expected if the combustor noise passes through the turbine to the respective nozzle exits.

CONCLUDING REMARKS

The problem of determining the source of noise emanating from aircraft turbine engines is difficult because of the many possible sources and their close proximity to each other. The two major sources, for turbofan engines at high engine operating speeds are probably the fan and the jet mixing noise. At low engine speeds the jet mixing and fan noise sources diminish in strength exposing other noise sources. It has been shown for low engine speeds that the broadband overall acoustic power level in the jet noise spectral region deviates from the jet noise prediction indicating that noise other than jet noise has become dominant. The noise generated by the combustion process has received considerable attention over the years. At present it appears that a simple theory may be used to predict the fluctuating pressure levels in aircraft type combustors. The theory indicates that the combustor contribution decreases as frequency increases. The derivation of the combustion noise theory of reference 25 showed that the cause of the combustion noise is the interaction of the fluctuating density due to turbulence with the mean energy gradient introduced by the burning process in the combustor. Realizing that the mean energy gradient may be either positive, as with the burning process, or negative, as with the work extracted from the hot gases by the turbine, one should expect that the turbine will produce a low frequency pressure fluctuation. In this experimental work coherence analysis has shown a general coherence between the combustor and far field signals at low frequencies. At frequencies between 200 and 600 Hz, just above the combustor-far field coherence region the turbine-far field coherence function shows a coherence level that cannot be neglected when compared to the combustor-far field coherence level. The significant differences in coherence function between the combustor-far field and turbine-far field coherence indicate that the turbine may be a source of noise in the frequency range between 200 and 600 Hz.

CONCLUSIONS

A quiet, clean, general aviation turbofan engine with two nozzle configurations, has been tested over a range of engine speeds. The engine nozzle configurations were an internal mixer nozzle and a separate flow coaxial nozzle. Internal fluctuating pressure measurements were made simultaneously in the combustor, turbine exit duct, nozzle and far field. The following conclusions have been drawn from analysis of these measured fluctuating pressures:

(1) The overall fluctuating pressure level in the test engine combustor has been predicted accurately from theory.

(2) The fluctuating pressure signals in the combustor, and at the turbine and core nozzle exit measuring stations, are partially correlated with the far field acoustic measurements, the correlation being greater at low engine speeds.

(3) In addition to again showing the contribution of combustion noise to far field noise the results also suggest an appreciable contribution from the turbine to the far field broadband noise in the low frequency range. A theoretical basis for the mechanism of this noise was postulated in the concluding remarks section.

APPENDIX A - LOW FREQUENCY NARROWBAND SPECTRA

The narrowband spectra from 0 to 2000 Hz for the fluctuating pressures measured in the combustor, turbine exit duct and in the far field at the 120°, 24.4 meter (80 ft) radius over the range of operating speeds are given in this Appendix. The spectra for both the separate flow (figs. A1 to A3), and mixer nozzles (fig. A4 to A6), are presentd. The pressures have not been corrected for the sensor environmental pressure but are given herein as output by the fast Fourier transform spectral analyzer. The 400 line spectra yield a frequency bandwidth of 5 Hz for the 0 to 2000 Hz frequency range presented herein.

APPENDIX B - LOW FREQUENCY COHERENCE FUNCTIONS

The low frequency ordinary coherence functions to a frequency of 1000 Hz have been determined for the QCGAT engine sensors for both the separate flow, (figs. B1 and B2), and mixer nozzle, (fig. B3 and B4), engine configurations. The functions are presented at engine speeds of 40 and 89 percent of maximum. The coherence signals are paired as follows:

(1) Combustor - turbine exit.
(2) Combustor - core nozzle exit (separate flow nozzle configuration).
(3) Combustor - mixer nozzle exit (mixer nozzle configuration).
(4) Combustor - 120°, 24.4 meter radius far field microphone.
(5) Turbine exit - core nozzle exit (separate flow nozzle configuration).
(6) Turbine exit - mixer nozzle exit (mixer nozzle configuration).
(7) Turbine exit - 120°, 24.4 meter radius far field microphone.
(8) Core nozzle exit - 120°, 24.4 meter radius far field microphone.
(9) Mixer nozzle exit - 120°, 24.4 meter radius far field microphone.

The separate flow nozzle engine configuration coherence functions are presented first for the 40 and 89 percent engine speeds, (figs. B1 and B2), and then the mixer nozzle engine configuration, (figs. B3 and B4).

Coherence functions less than unity but not zero may be the result of a third noise source being present. Coherence functions of close to unity show a great similarity of the two signals and probably means the signals are from the same source. A zero coherence function suggests that the signals share nothing in common. The coherence functions given herein were obtained with a bandwidth of 2 Hz and were the result of 2×10^9 averages.

REFERENCES

1. Huff, R. G.; Clark, B. J.; and Dorsch, R. G.: Interim Prediction Method for Low Frequency Core Engine Noise. NASA TM X-71627, 1974.
2. Doyle, V. L.; and Moore, M. T.: Core Noise Investigation of the CF6-50 Turbofan Engine, Final Report. (R79AEG395, General Electric Co.; NASA Contract NAS3-21260.) NASA CR-159749, 1980.
3. Woodward, R. P.; and Minner, G. L.: Low-Frequency Rear Quadrant Noise of a Turbojet Engine with Exhaust Duct Muffling. NASA TM X-2718, 1973.
4. Mathews, D. C.; and Peracchio, A. A.: Progress in Core Engine and Turbine Noise Technology. AIAA Paper 74-948, August 1974.
5. Karchmer, A. M.; and Reshotko, M.: Core Noise Source Diagnostics on a Turbofan Engine Using Correlation and Coherence Techniques. NASA TM X-73535, 1976.
6. Reshotko, M.; and et al.: Core Noise Measurements on a YF-102 Turbofan Engine. AIAA Paper 77-21, NASA TM X-73587, 1977.
7. Karchmer, A. M.; Reshotko, M.; and Montegani, F. J.: Measurement of Far Field Combustion Noise from a Turbofan Engine Using Coherence Functions. NASA TM-73748, 1977.
8. Reshotko, M.; and Karchmer, A.: Combustor Fluctuating Pressure Measurements in Engine and in a Component Test Facility: A Preliminary Comparison. NASA TM-73845, 1977.
9. Bilwakesh, K. R.; and et al.: Core Engine Noise Control Program. Volumes I, II and III. FAA-RD-74-125, General Electric, 1974. (Vol. I, AD-A013128/4; Vol. II, AD-A013129/2; Vol. III, AD-A013131/8.)
10. Matta, R. K.; Sandusky, G. T.; and Doyle, V. L.: GE Core Engine Noise Investigation, Low Emission Engines. FAA-RD-77-4, General Electric Co., 1977. (AD-A048590.)
11. Mathews, D. C.; Rekos, N. F., Jr.; and Nagel, R. T.: Combustion Noise Investigation - Predicting Direct and Indirect Noise from Aircraft Engine. FAA-RD-77-3, Pratt and Whitney Aircraft Group., 1977. (AD-A038154/1.)
12. von Glahn, U. H.: Correlation of Combustor Acoustic Power Levels Inferred from Internal Fluctuating Pressure Measurements. NASA TM-78986, 1978.
13. Reshotko, M.; and Karchmer, A.: Core Noise Measurements from a Small, General Aviation Turbofan Engine. NASA TM-81610, 1980.
14. Emmerling, J. J.: Experimental Clean Combustor Program, Noise Measurement Addendum, Phase I. (GE75AEG315, General Electric Co., NASA Contract NAS3-16830.) NASA CR-134853, 1975.
15. Sofrin, T. G.; and Ross, D. A.: Noise Addendum Experimental Clean Combustor Program, Phase I. (PWA-5252, Pratt and Whitney Aircraft; NASA Contract NAS3-16829.) NASA CR-134820, 1975.
16. Emmerling, J. J.; and Bekofske, K. L.: Experimental Clean Combustor Program; Noise Measurement Addendum, Phase II. (R75AEG147-13-ADD, General Electric Co.; NASA Contract NAS3-18551.) NASA CR-135045, 1976.
17. Sofrin, T. G.; and Riloff, N., Jr.: Experimental Clean Combustor Program: Noise Study. (PWA-5458, Pratt and Whitney Aircraft; NASA Contract NAS3-18544.) NASA CR-135106, 1976.
18. Doyle, V. L.: Experimental Clean Combustor Program, Phase III: Noise Measurement Addendum. (R78AEG319, General Electric Co.; NASA Contract NAS3-19736.) NASA CR-159458, 1978.
19. Doyle, V. L.: Core Noise Investigation of the CF6-50 Turbofan Engine. (R79AEG247, General Electric Co.; NASA Contract NAS3-21260.) NASA CR-159598, 1980.

20. Wilson, C. A.: YF102 In-Duct Combustor Noise Measurement. Vol. I, II and III. (LYC-77-56, Avco Lycoming Div.; NASA Contract NAS3-20052.) NASA CR-135404, 1977.
21. Burdsall, E. A.; Brochu, F. P.; and Scaramella, V. M.: Results of Acoustic Testing of the JT8D-109 Refan Engines. (PWA-5298, Pratt and Whitney Aircraft; NASA Contract NAS3-17840.) NASA CR-134875, 1975.
22. Muthukrishnan, M.; Strahle, W. C.; and Handley, J. C.: The Effect of Flame Holders on Combustion Generated Noise. AIAA Paper 76-39, Jan., 1976.
23. Stephenson, J.; and Hassan, H. A.: The Spectrum of Combustion-Generated Noise. J. of Sound and Vib., vol. 53, July 22, 1977, pp. 283-288.
24. Mahan, J. R.; and Kasper, J. M.: Influence of Heat Release Distribution on the Acoustic Response of Long Burners. ASME Paper 79-DET-31, Sept. 1979.
25. Huff, Ronald G.: A Simplified Combustion Noise Theory Yielding a Prediction of Fluctuating Pressure Level. NASA TP-2237, 1984.
26. Heldenbrand, R. W.; and Norgren, W. M.: AiResearch QCGAT Program-Quiet Clean General Aviation Turbofan Engines. (AIRESEARCH-21-3071, AiResearch Mfg. Co.; NASA Contract NAS3-20585.) NASA CR-159758, 1979.
27. Krejsa, E. A.; and Karchmer, A. M.: Acoustic Modal Analysis of the Pressure Field in the Tailpipe of a Turbofan Engine. NASA TM-83387, 1983.

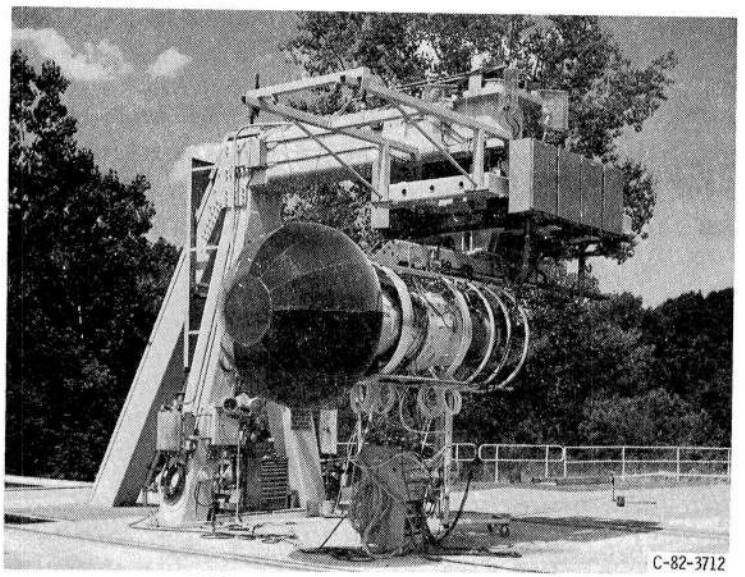

(a) Front view of inlet screen installed.

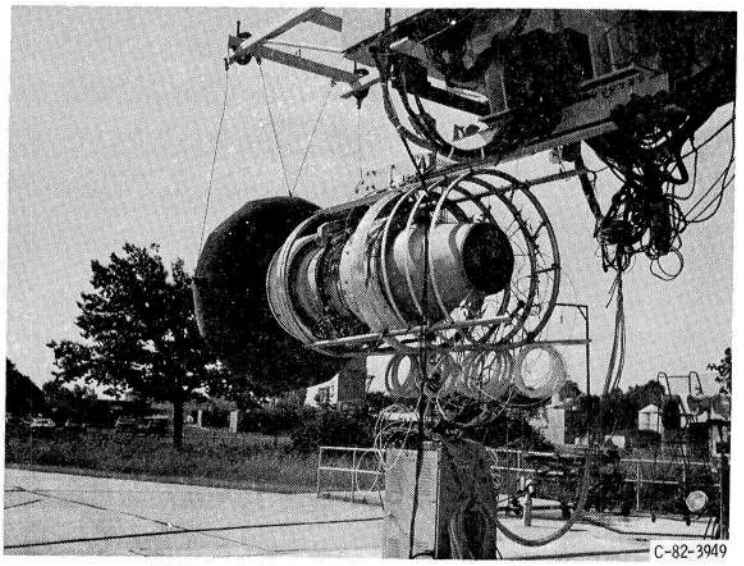

(b) Separate-flow nozzle engine configuration.

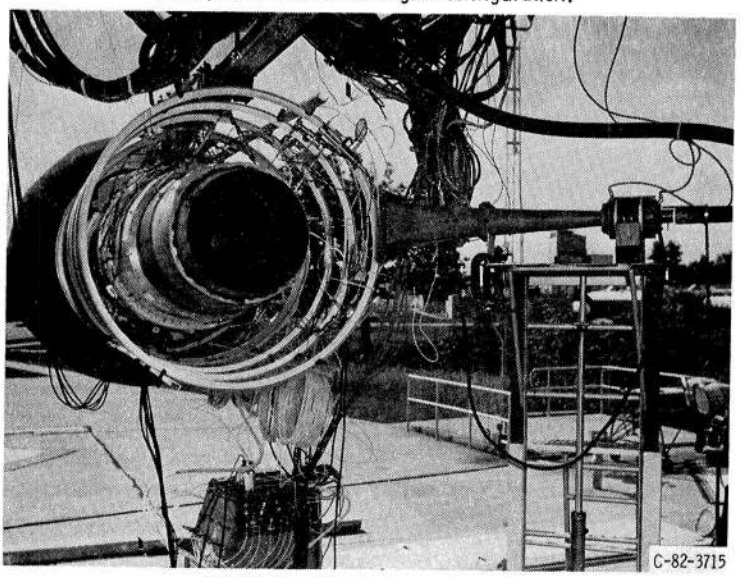

(c) Mixer nozzle engine configuration.

Figure 1. - QCGAT Engine installed in vertical lift fan test facility.

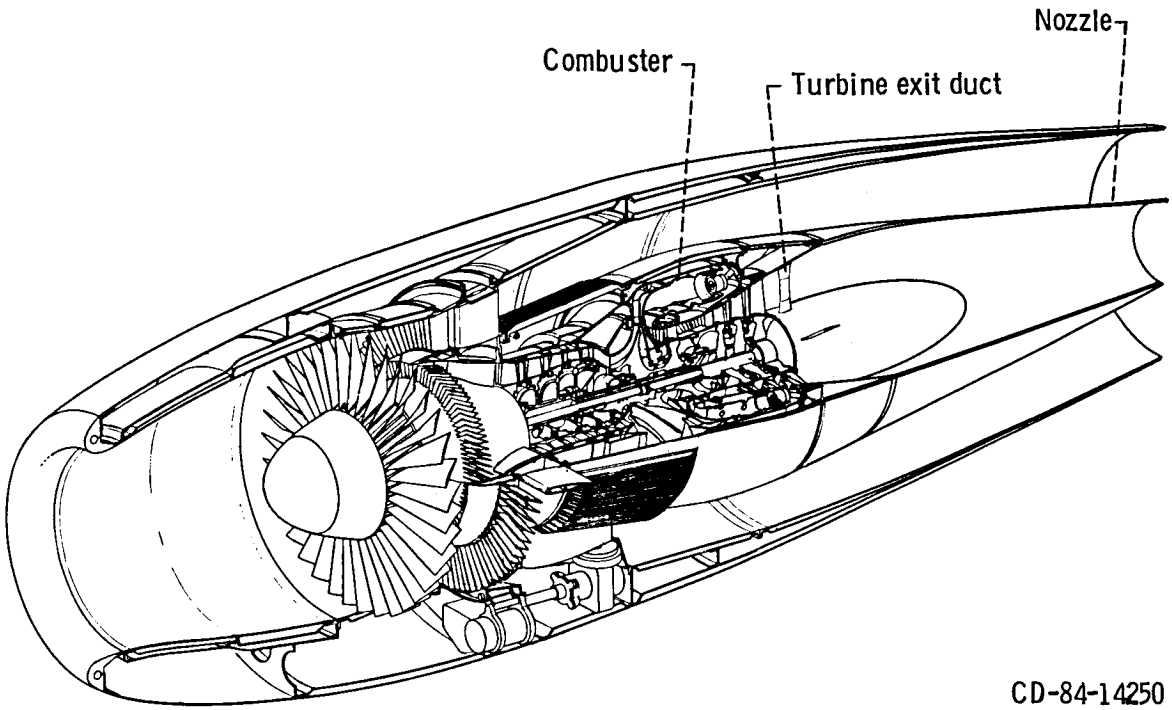

(a) Separate-flow nozzle

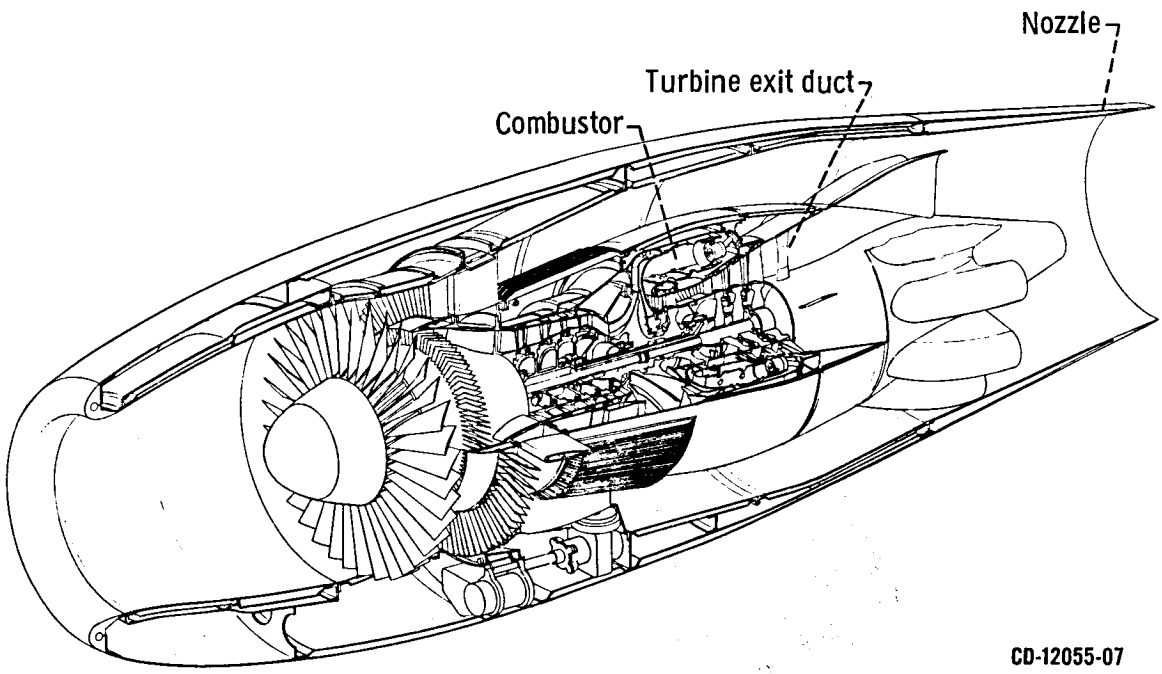

(b) Mixer nozzle engine configuration.

Figure 2. - Isometric view of engine and instrumentation.

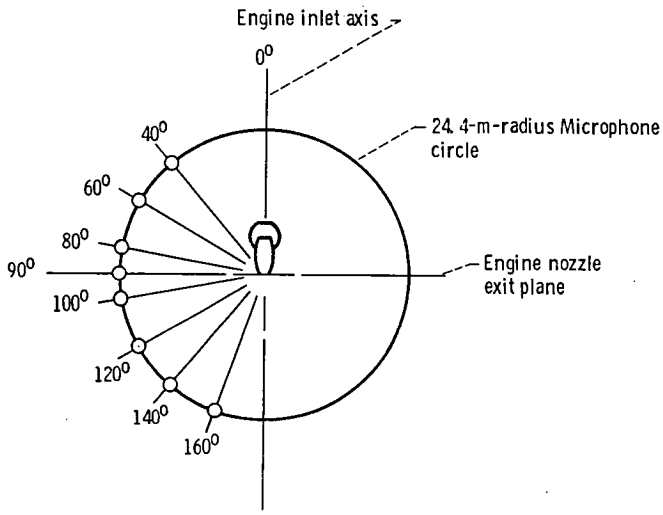

Figure 3. - Far-field microphone layout for QCGAT core noise test at ground level. (Engine is 2.9 m above ground plane.)

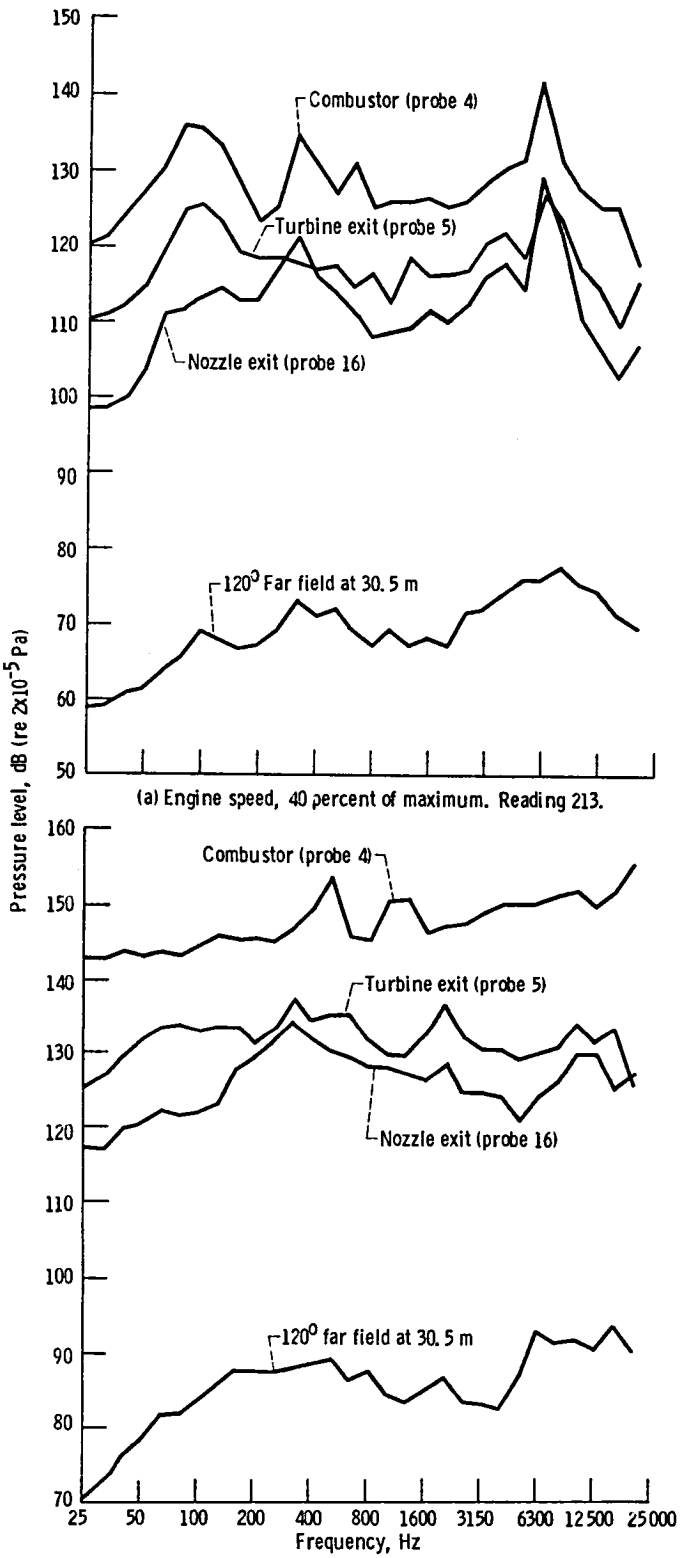

(a) Engine speed, 40 percent of maximum. Reading 213.

(b) Engine speed, 89 percent of maximum. Reading 219.

Figure 4. - QCGAT internal and far-field 1/3-octave pressure spectra for separate-flow nozzle. Test AQ4-6; probe data corrected for environment (i.e., microphone atmospheric pressure).

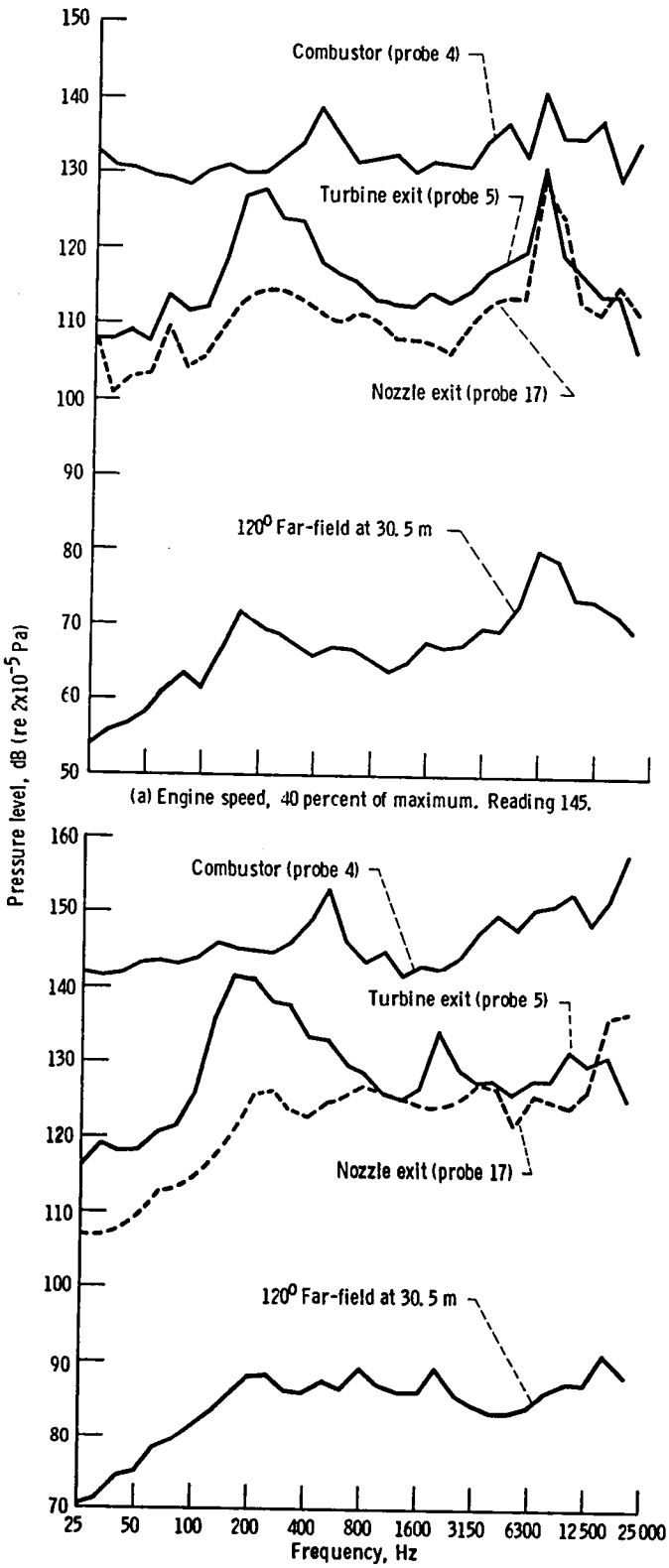

(a) Engine speed, 40 percent of maximum. Reading 145.

(b) Engine speed, 89 percent of maximum. Reading 152.

Figure 5. - QCGAT internal and far-field 1/3-octave pressure spectra for mixer nozzle. Test AQ4-1; probe corrected for environment (i.e., microphone atmospheric pressure).

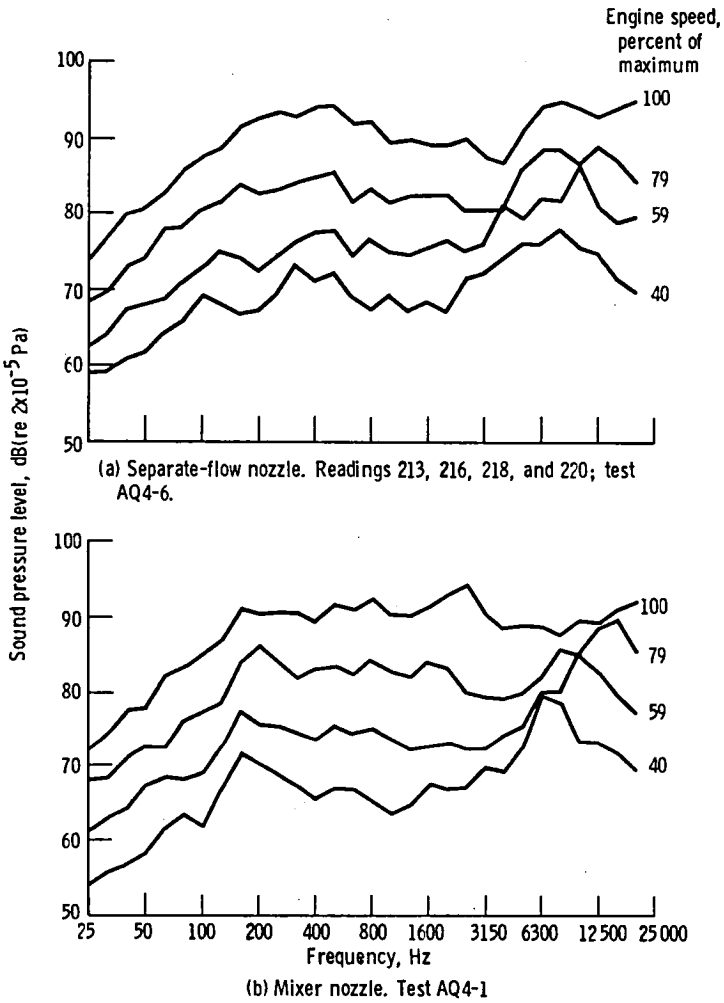

(a) Separate-flow nozzle. Readings 213, 216, 218, and 220; test AQ4-6.

(b) Mixer nozzle. Test AQ4-1

Figure 6. - Far-field acoustic 1/3-octave pressure spectra. Distance, 50.5 m; 120° from engine inlet axis.

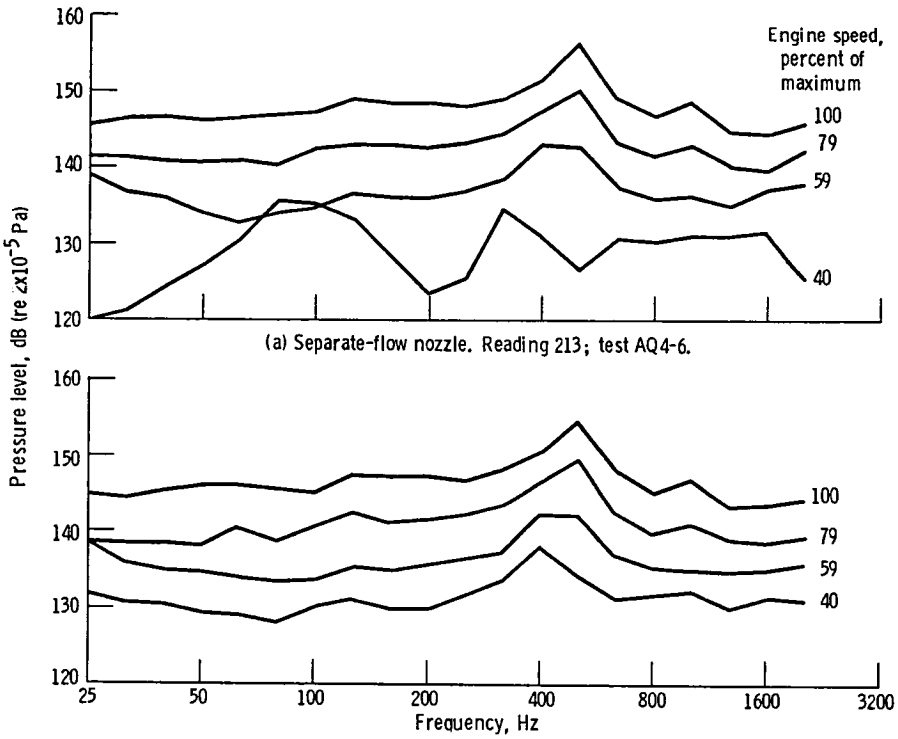

(a) Separate-flow nozzle. Reading 213; test AQ4-6.

(b) Mixer nozzle. Reading 145; test AQ4-1.

Figure 7. - One-third-octave combustor pressure spectra as function of engine speed. Probe 4.

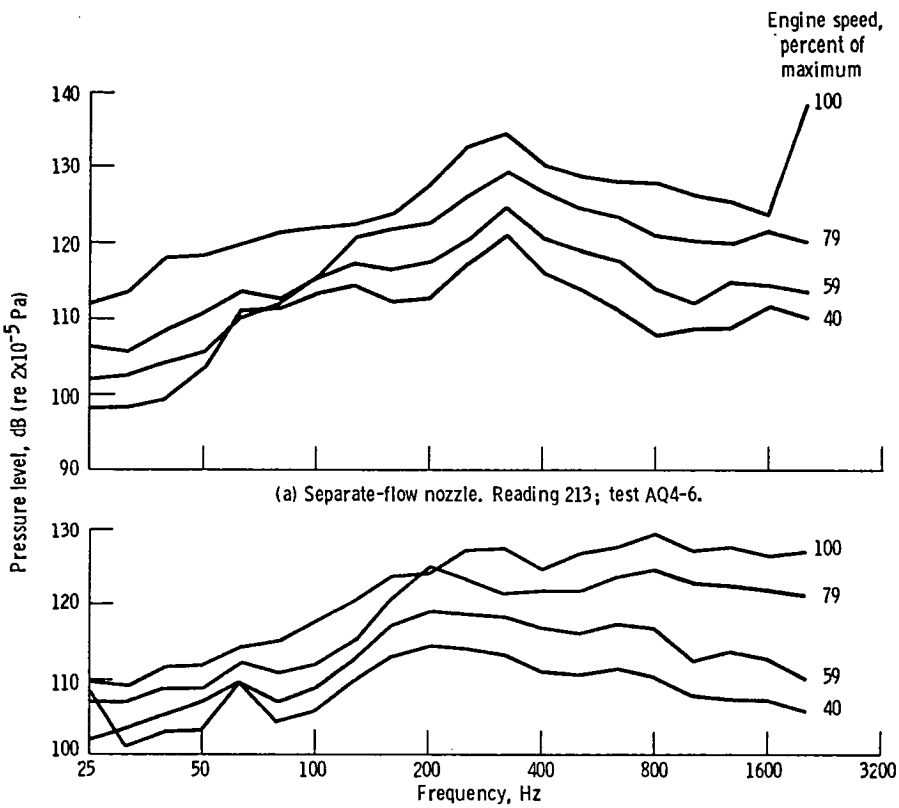

(a) Separate-flow nozzle. Reading 213; test AQ4-6.

(b) Mixer nozzle. Reading 145; test AQ4-1.

Figure 8. - Tailpipe duct 1/3-octave pressure spectra as function of engine speed.

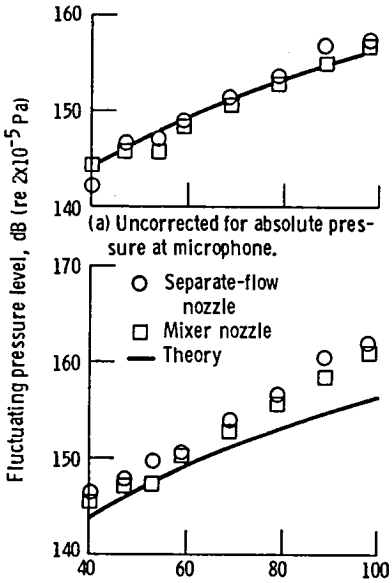

Figure 9. - Combustor fluctuating pressure level theory and measured values as function of engine speed.

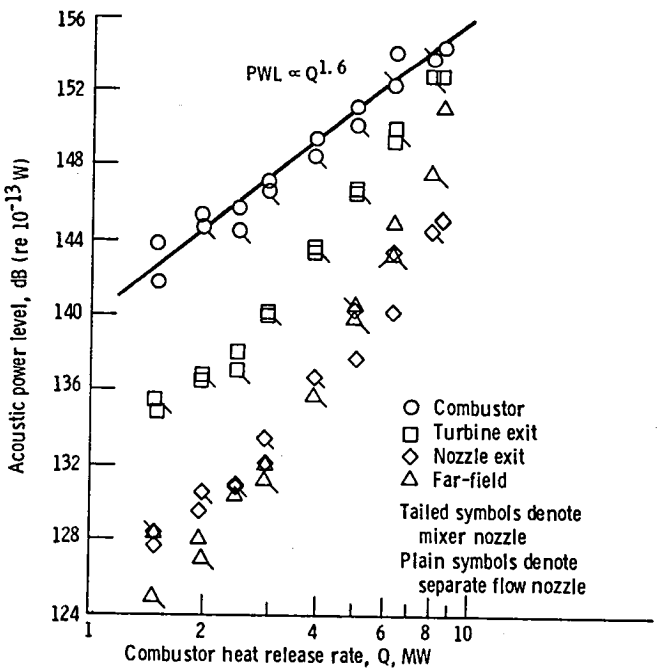

Figure 10. - Acoustic power as function of heat release rate. Frequency range, 25 to 2000 Hz.

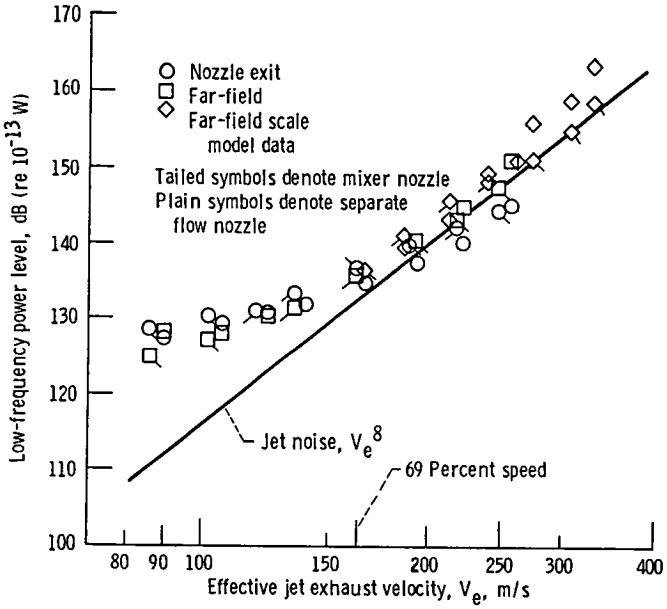

Figure 11. - QCGAT low-frequency acoustic power. Frequency range, 25 to 2000 Hz.

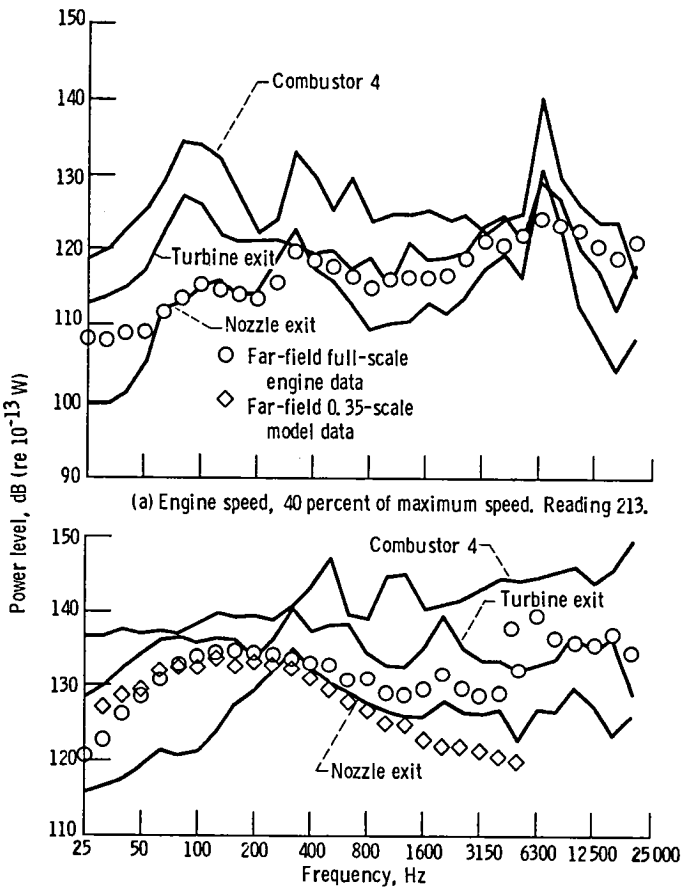

Figure 12. - QCGAT internal and far-field power level spectra for separate-flow nozzle. Test AQ4-6.

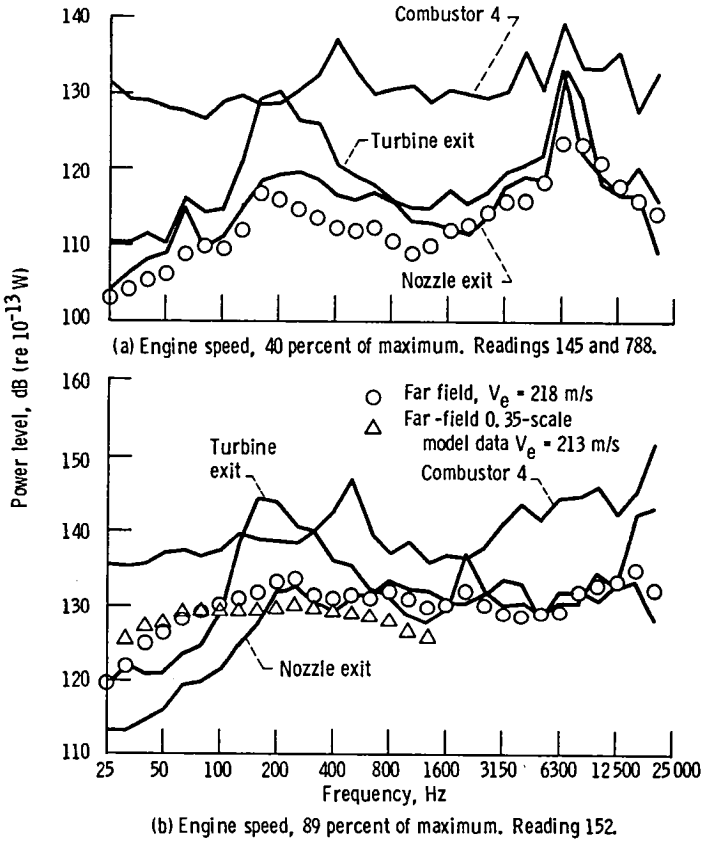

(a) Engine speed, 40 percent of maximum. Readings 145 and 788.

(b) Engine speed, 89 percent of maximum. Reading 152.

Figure 13. - QCGAT internal and far-field power spectra for mixer nozzle. Test AQ4-1.

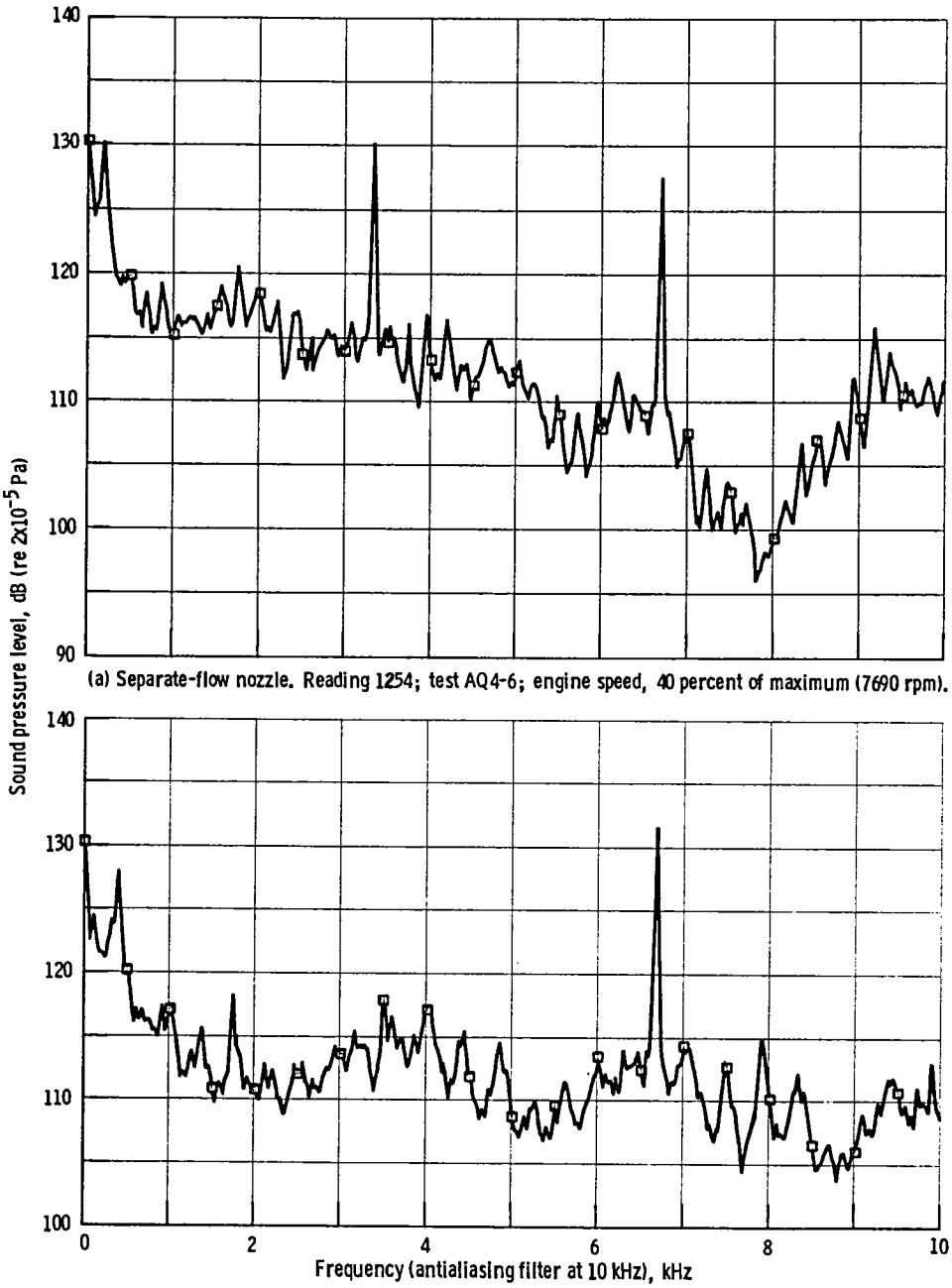

(a) Separate-flow nozzle. Reading 1254; test AQ4-6; engine speed, 40 percent of maximum (7690 rpm).

(b) Mixer nozzle. Reading 1197; test AQ4-1; engine speed, 40 percent of maximum (7640 rpm).

Figure 14. - Combustor narrow-band pressure spectra. Probe 4; bandwidth, 25 Hz; average of 64 samples.

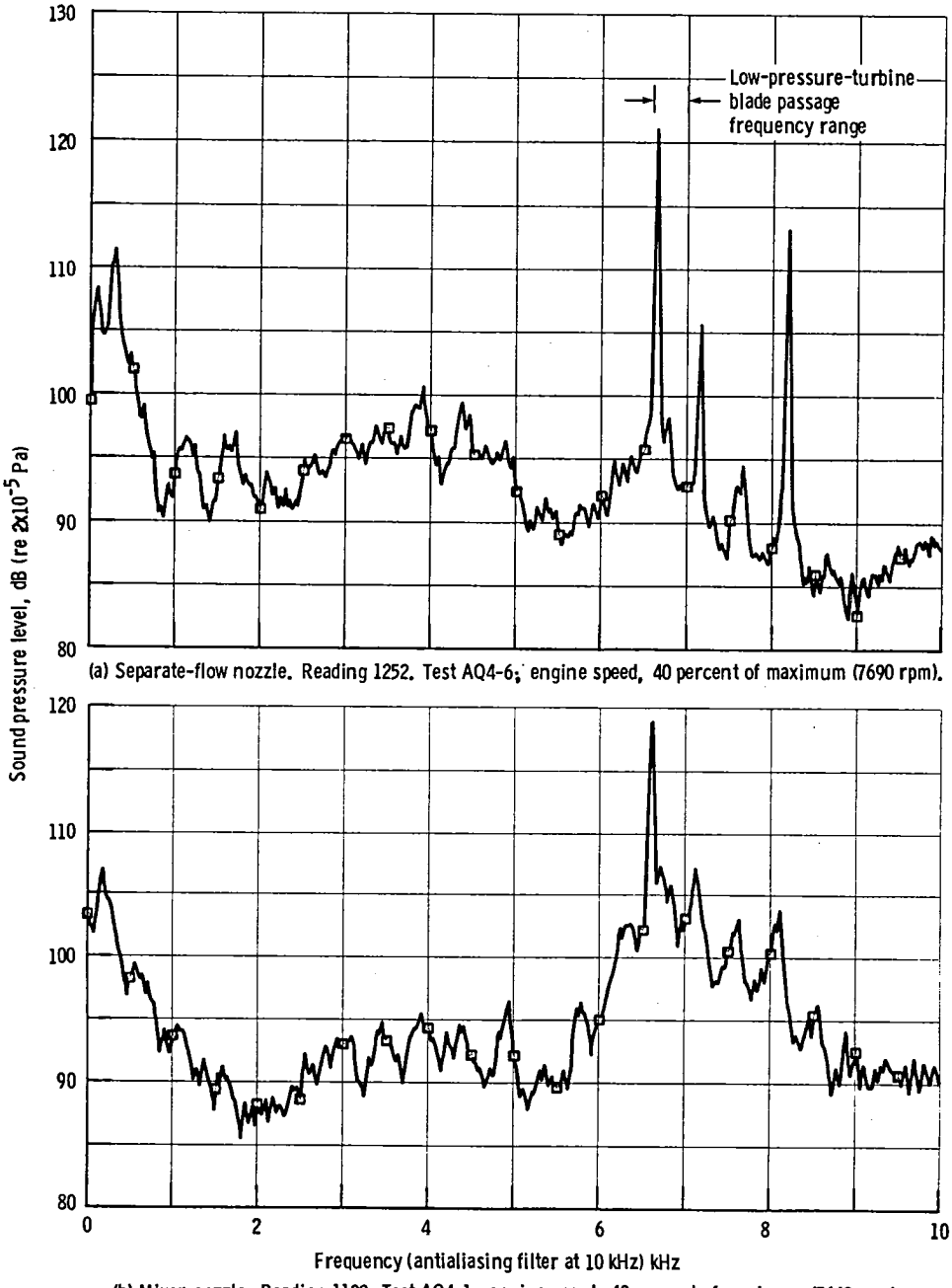

(a) Separate-flow nozzle. Reading 1252. Test AQ4-6; engine speed, 40 percent of maximum (7690 rpm).

(b) Mixer nozzle. Reading 1199. Test AQ4-1; engine speed, 40 percent of maximum (7640 rpm).

Figure 15. - Nozzle narrow-band pressure spectra. Probe 17; bandwidth, 25 Hz; average of 64 samples.

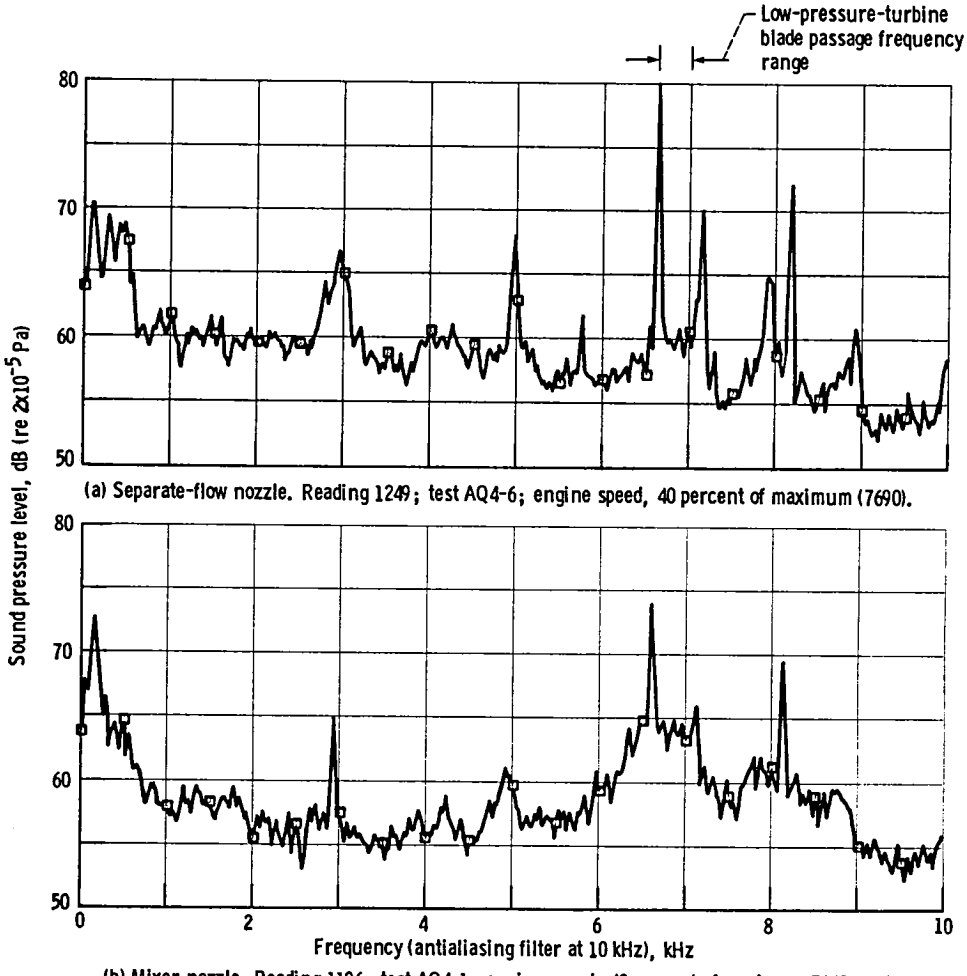

(a) Separate-flow nozzle. Reading 1249; test AQ4-6; engine speed, 40 percent of maximum (7690).

(b) Mixer nozzle. Reading 1196; test AQ4-1; engine speed, 40 percent of maximum 7640 rpm).

Figure 16. - Far-field narrow-band 120^{0} sound pressure level spectra to 10 kHz; bandwidth, 25 Hz; average of 64 samples.

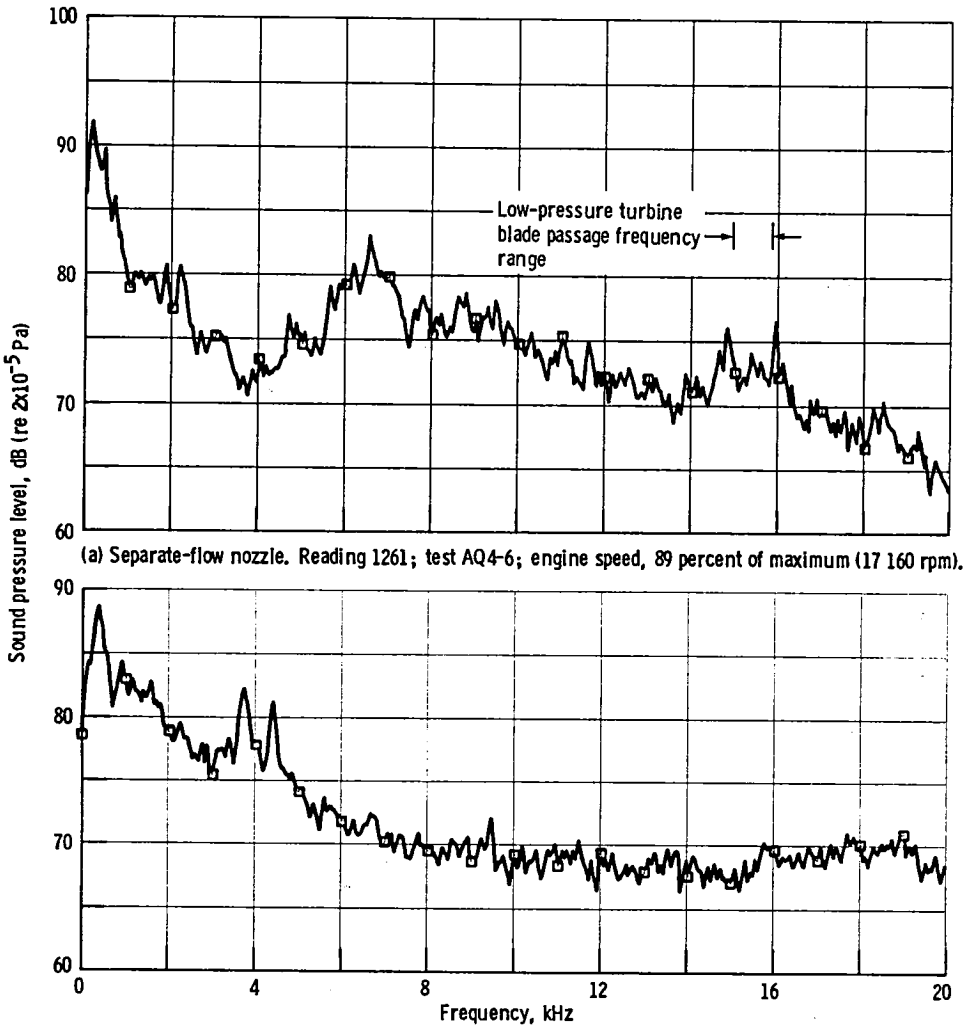

(a) Separate-flow nozzle. Reading 1261; test AQ4-6; engine speed, 89 percent of maximum (17 160 rpm).

(b) Mixer nozzle. Reading 1204; test AQ4-1; engine speed, 89 percent of maximum (17 060 rpm).

Figure 17. - Far-field narrow-band 120° sound pressure level spectra to 20 kHz; bandwidth, 50 Hz; average of 64 samples.

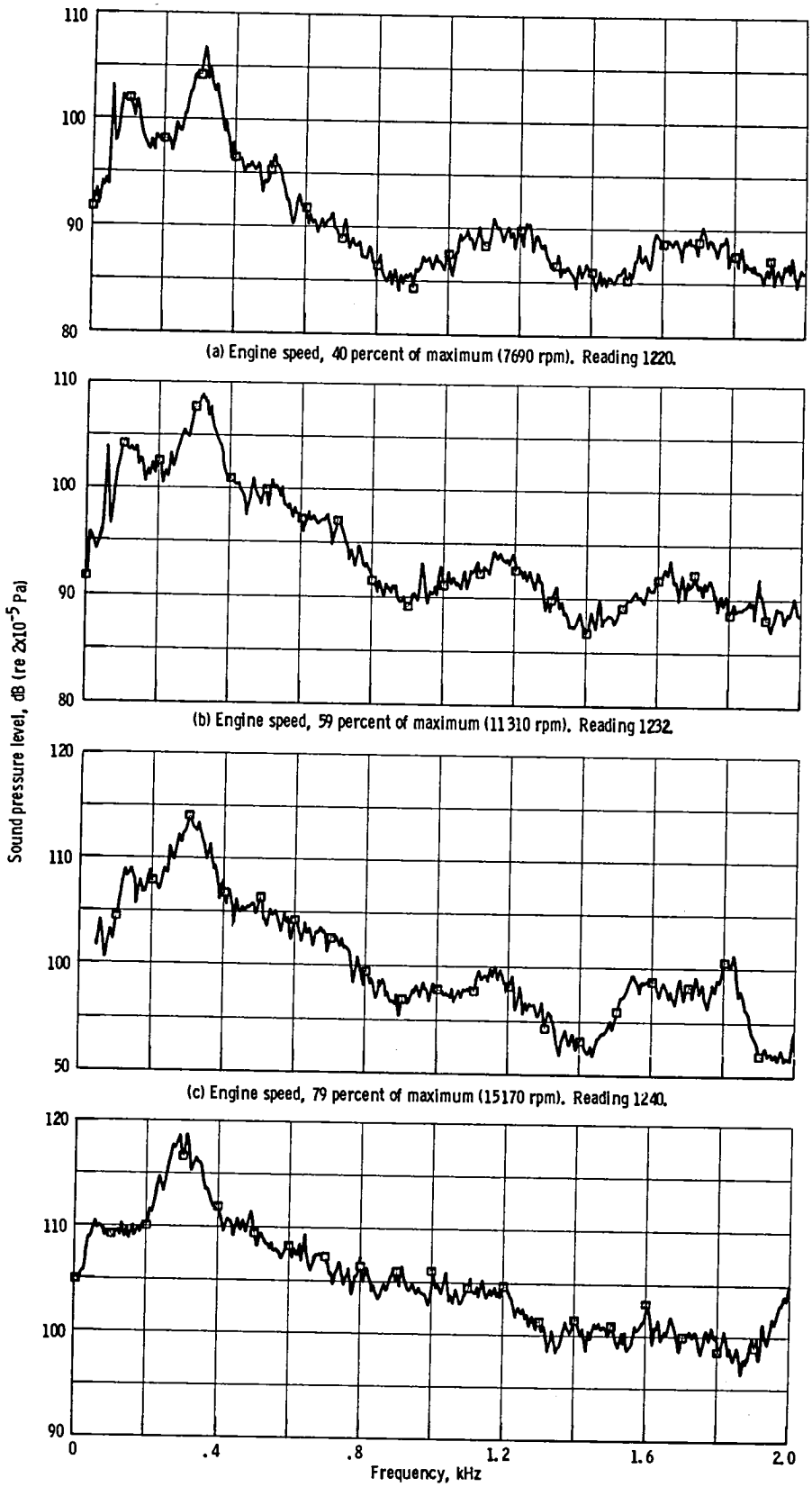

Figure 18. - Nozzle low-frequency narrow-band pressure spectra for separate-flow engine configuration. Probe 17; test AQ4-6; bandwidth, 5 Hz; average of 64 samples.

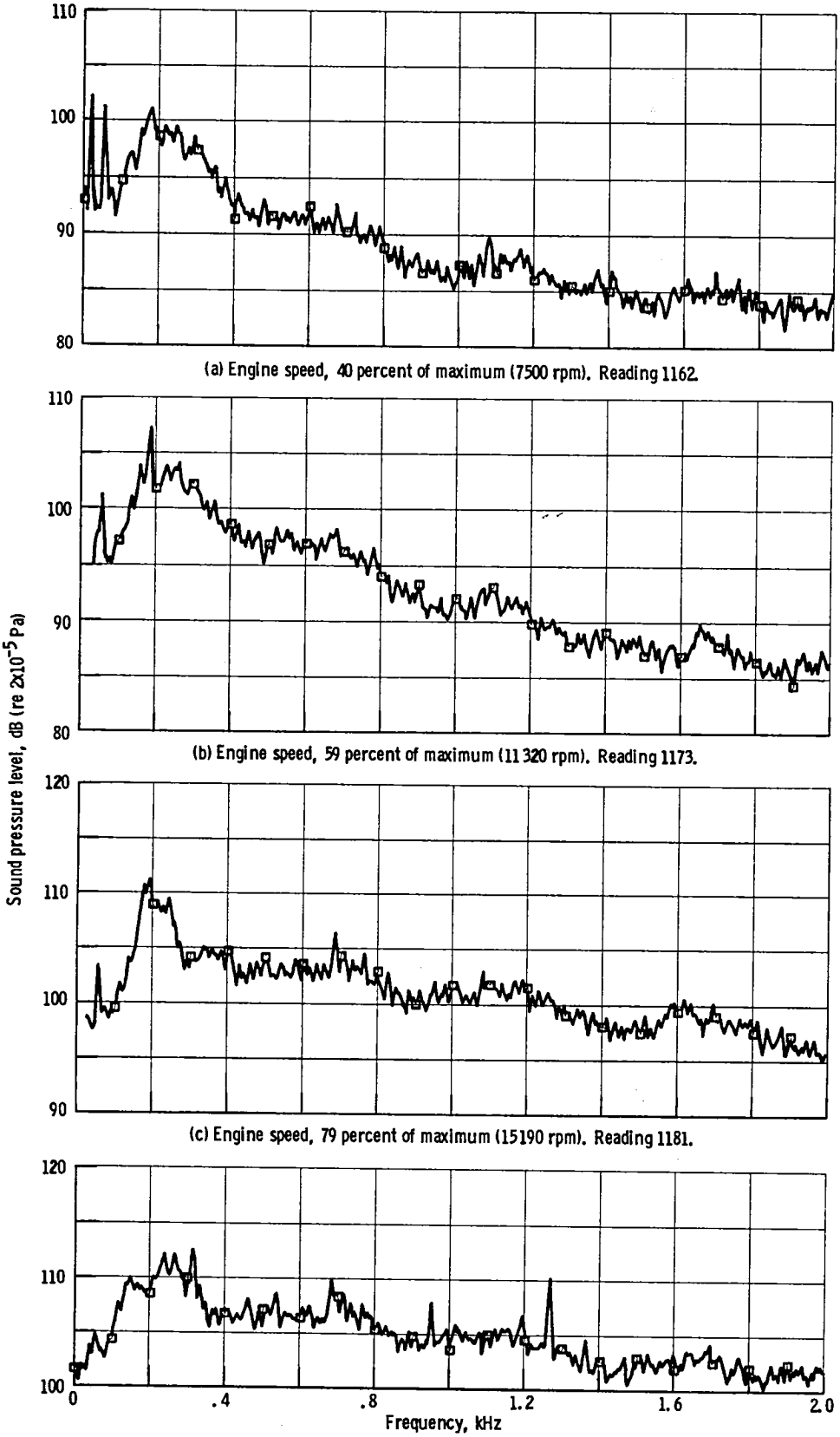

Figure 19. - Nozzle low-frequency narrow-band spectra for mixer nozzle engine configuration. Probe 17; test AQ4-1; bandwidth, 5 Hz; average of 64 samples.

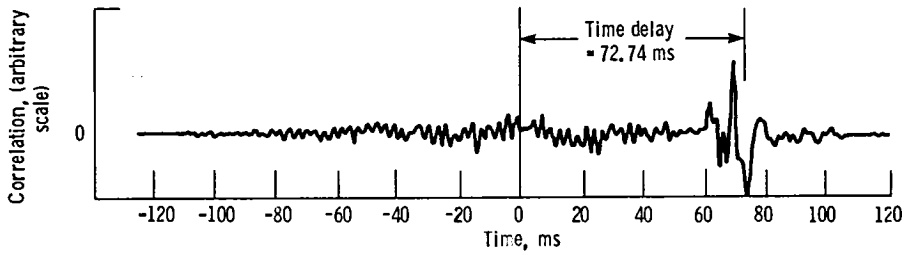

Figure 20. - Cross correlation between combustor and 120° far-field microphone pressure signals for separate-flow nozzle. Reading 213; test AQ4-6; engine speed, 40 percent of maximum; far-field microphone radius, 24.4 m; minimum discernible time delay, 0.2441 ms.

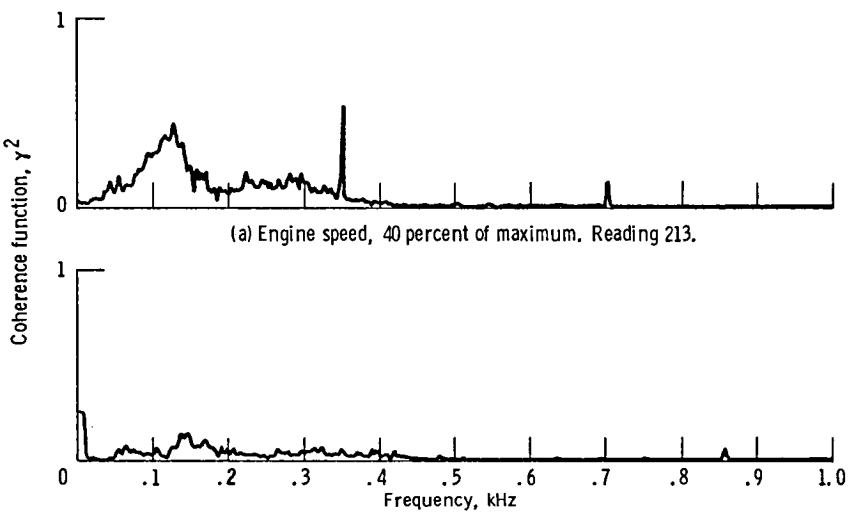

(a) Engine speed, 40 percent of maximum. Reading 213.

(b) Engine speed, 89 percent of maximum. Reading 219.

Figure 21. - Coherence function between combustor and 120° far-field microphone pressure signals for separate-flow nozzle engine configuration. Test AQ4-6; bandwidth, 2 Hz; tape channels 3 and 10. Number of averages in coherence analysis, N = 9.

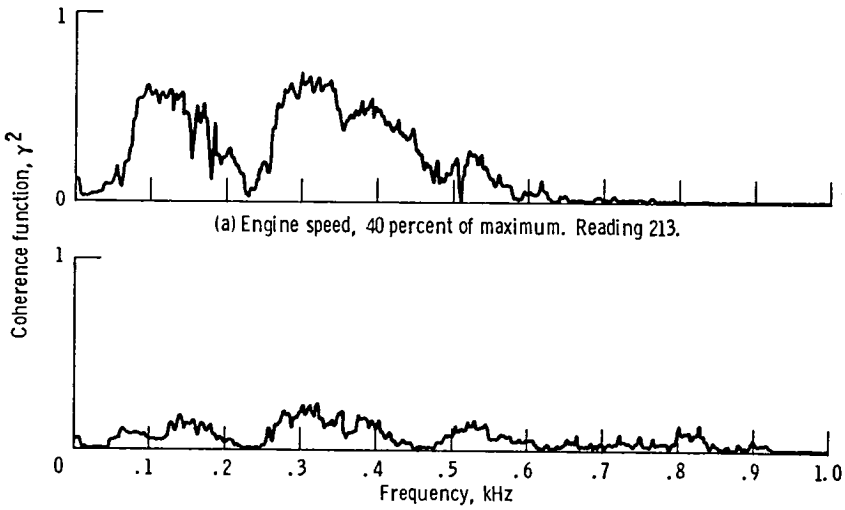

(a) Engine speed, 40 percent of maximum. Reading 213.

(b) Engine speed, 89 percent of maximum. Reading 219.

Figure 22. - Coherence function between turbine exit and 120° far-field microphone pressure signals for separate-flow nozzle engine configuration. Test AQ4-6; bandwidth, 2 Hz; tape channels 4 and 10. Number of averages in coherence analysis, N = 9.

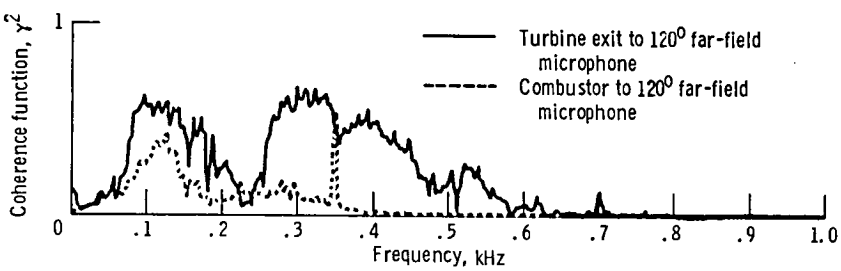

Figure 23. - Comparison of coherence function between combustor and turbine exit pressure signals to far-field microphone at 120° from engine inlet axis for separate-flow nozzle engine configuration. Engine speed, 40 percent of maximum.

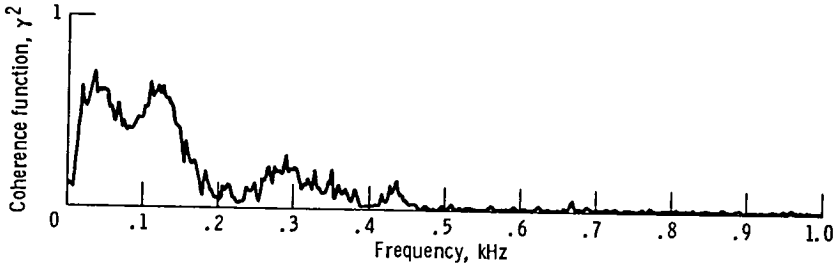

Figure 24. - Coherence function between combustor and turbine exit pressure signals for separate-flow nozzle engine configuration. Reading 213; test AQ4-6; engine speed, 40 percent of maximum; bandwidth, 2 Hz; tape channels 3 and 4; number of averages in coherence analysis, N = 6.

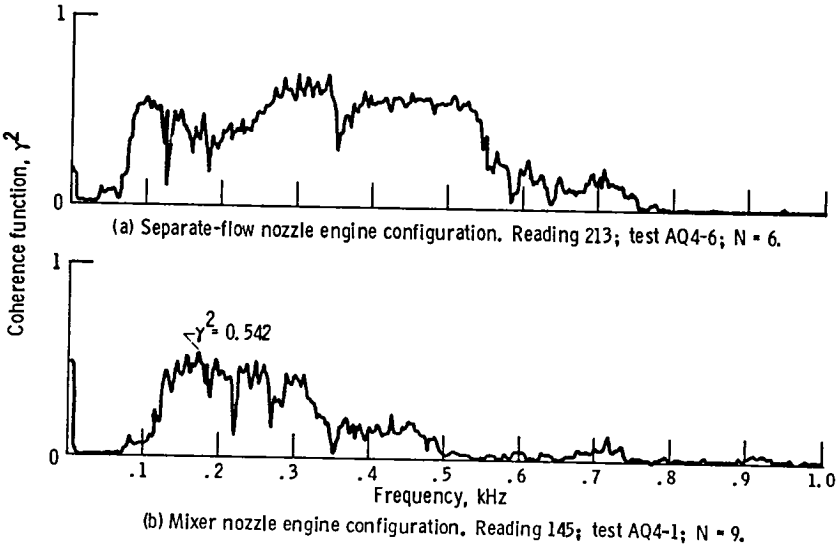

(a) Separate-flow nozzle engine configuration. Reading 213; test AQ4-6; N = 6.

(b) Mixer nozzle engine configuration. Reading 145; test AQ4-1; N = 9.

Figure 25. - Comparison of coherence function between nozzle exit and 120° far-field microphone pressure signals for separate-flow and mixer nozzle engine configurations. Engine speed, 40 percent of maximum; bandwidth, 2 Hz; tape channels 13 and 10.

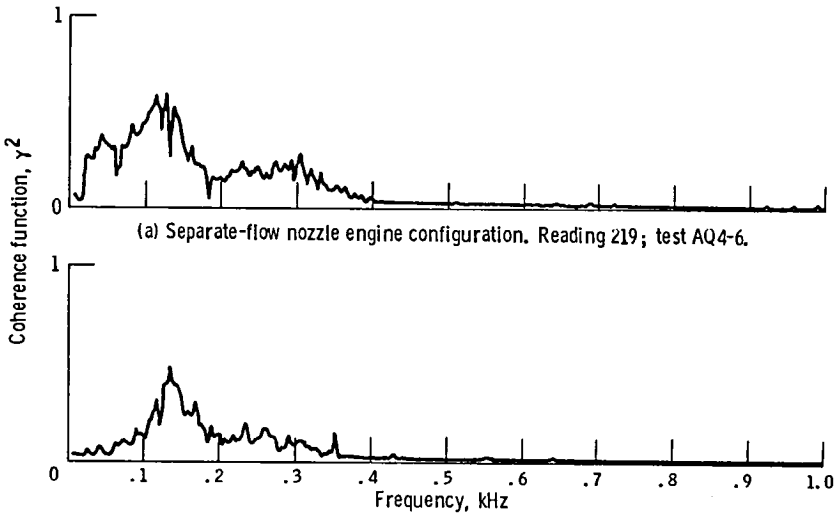

(a) Separate-flow nozzle engine configuration. Reading 219; test AQ4-6.

(b) Mixer nozzle engine configuration. Reading 145; test AQ4-1.

Figure 26. - Comparison of coherence function between combustor and nozzle exit pressure signals for separate-flow and mixer nozzle engine configurations. Engine speed, 40 percent of maximum; bandwidth 2 Hz; tape channels 3 and 13; number of averages in coherence analysis, N = 9.

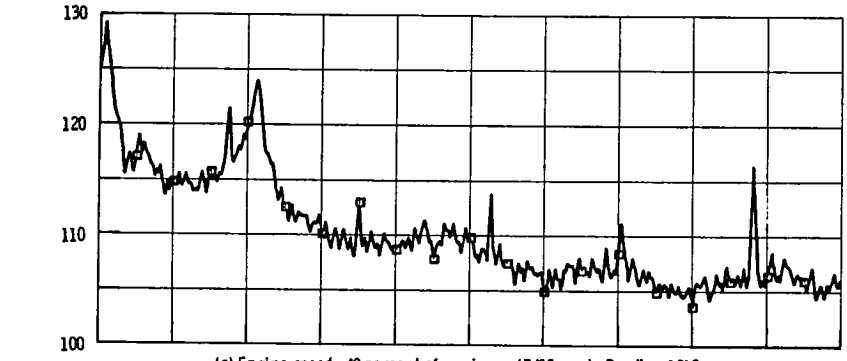

(a) Engine speed, 40 percent of maximum (7490 rpm). Reading 1218.

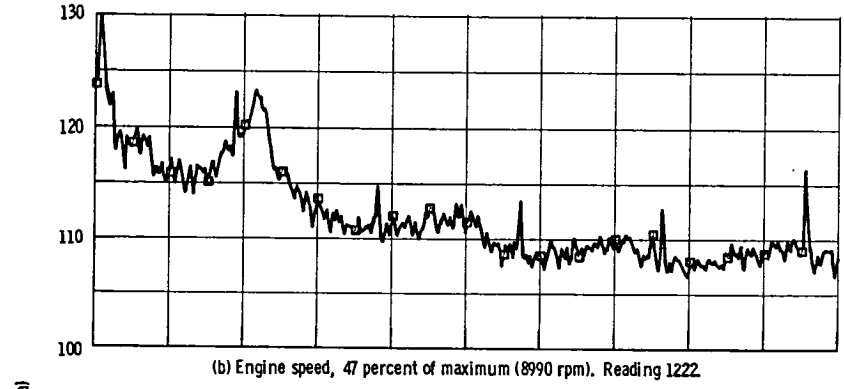

(b) Engine speed, 47 percent of maximum (8990 rpm). Reading 1222.

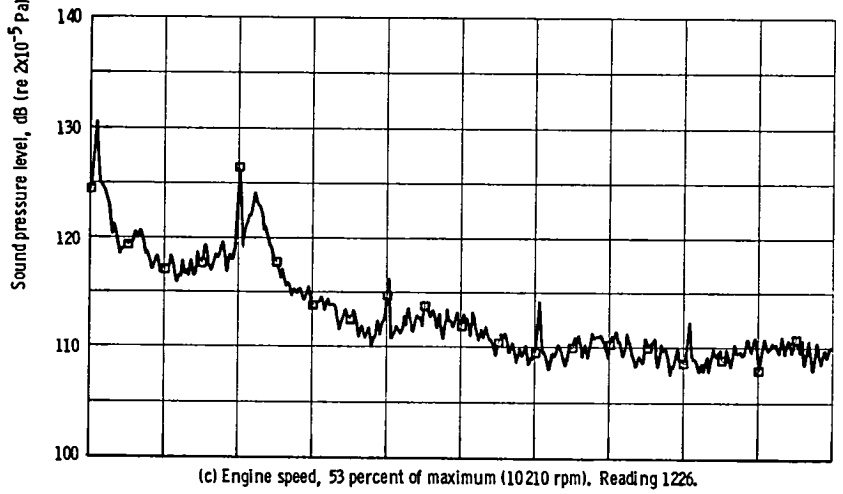

(c) Engine speed, 53 percent of maximum (10210 rpm). Reading 1226.

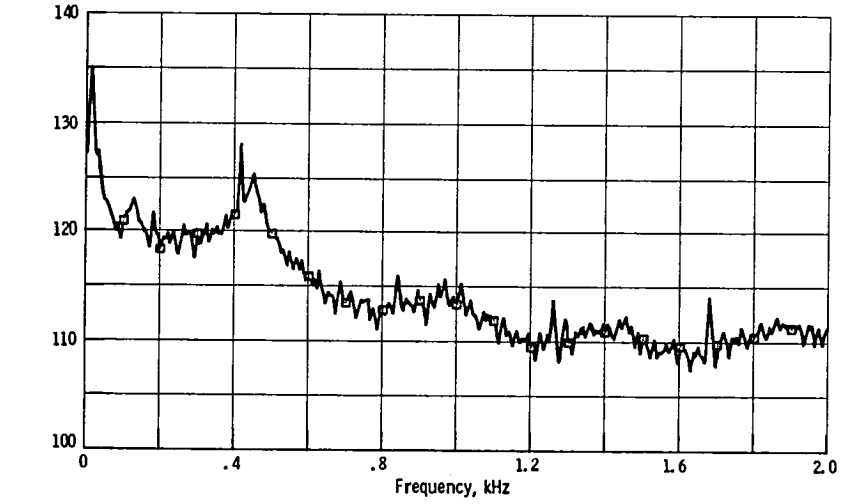

(d) Engine speed, 59 percent of maximum (11310 rpm). Reading 1230.

Figure A1. - Combustor pressure spectra for separate-flow nozzle engine configuration. Test AQ4-6; 64 average.

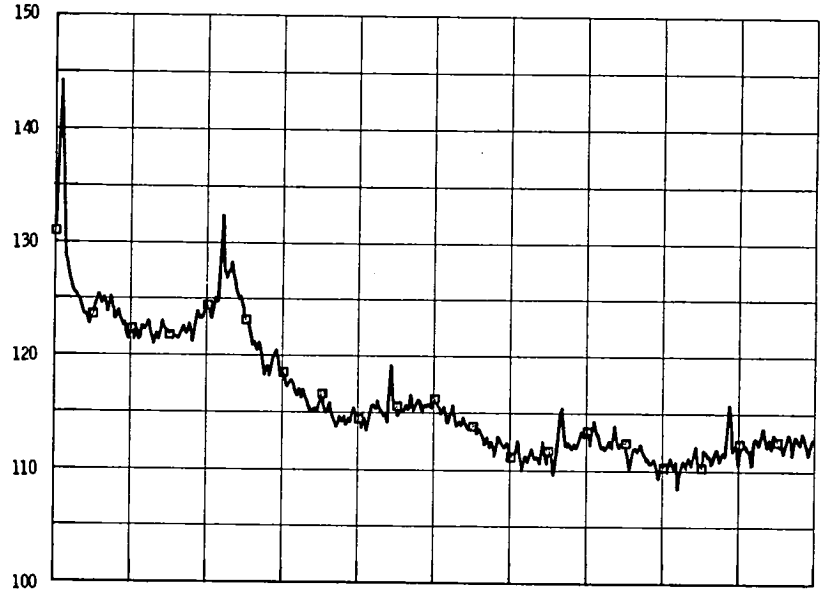

(e) Engine speed, 69 percent of maximum (13000 rpm). Reading 1234.

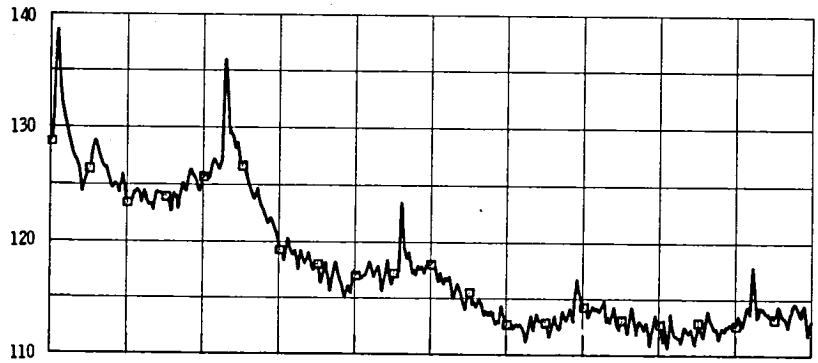

(f) Engine speed, 79 percent of maximum (15170 rpm). Reading 1238.

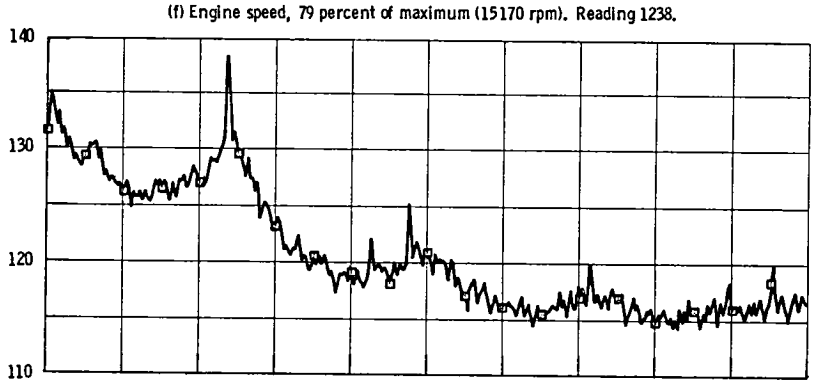

(g) Engine speed, 89 percent of maximum (17160 rpm). Reading 1242.

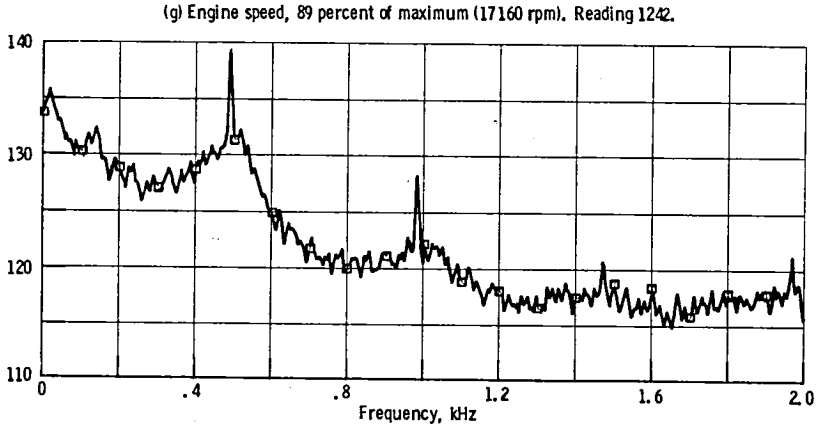

(h) Engine speed, 100 percent (18260 rpm). Reading 1246.

Figure A1. - Concluded.

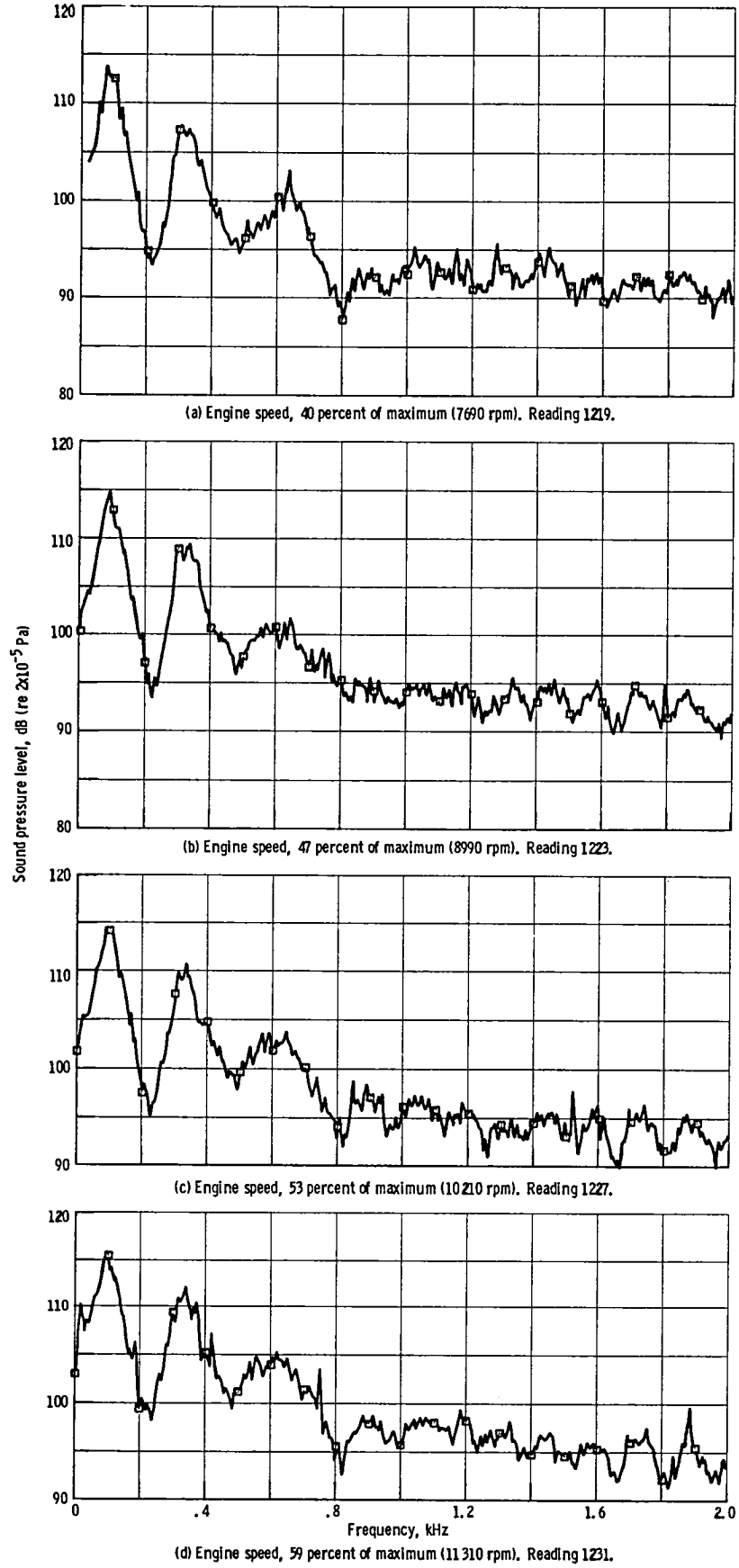

(a) Engine speed, 40 percent of maximum (7690 rpm). Reading 1219.

(b) Engine speed, 47 percent of maximum (8990 rpm). Reading 1223.

(c) Engine speed, 53 percent of maximum (10210 rpm). Reading 1227.

(d) Engine speed, 59 percent of maximum (11310 rpm). Reading 1231.

Figure A2. - Turbine exit pressure spectra for separate-flow nozzle engine configuration. Test AQ4-6; average of 64 samples.

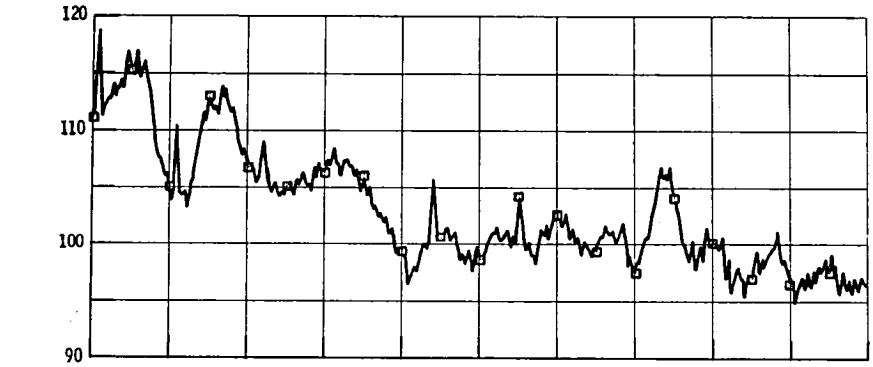

(e) Engine speed, 69 percent of maximum (13 290 rpm). Reading 1235.

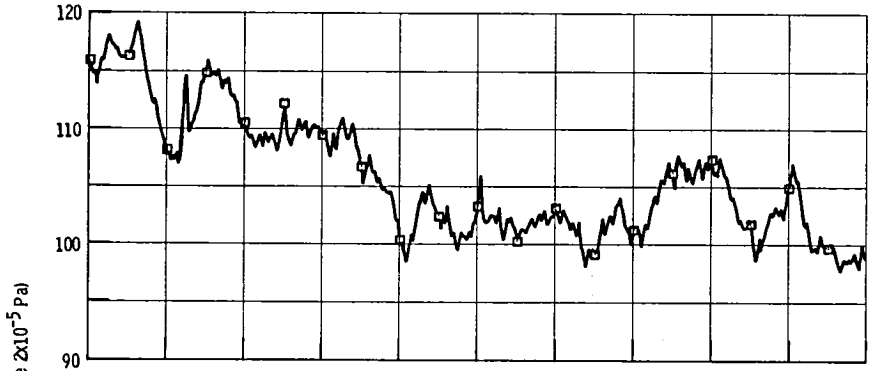

(f) Engine speed, 79 percent of maximum (15 170 rpm). Reading 1239.

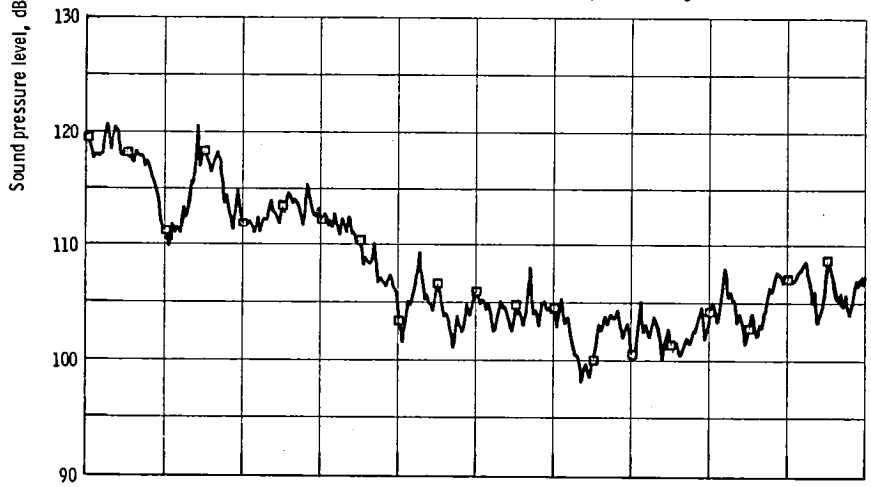

(g) Engine speed, 89 percent of maximum (17 160 rpm). Reading 1243.

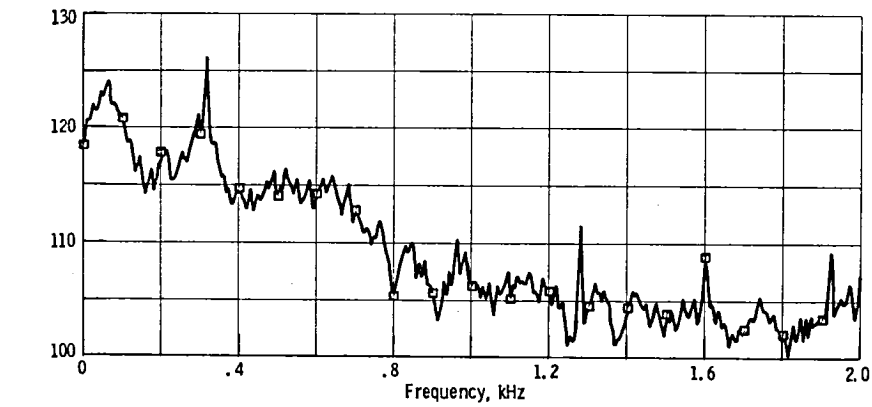

(h) Engine speed, 100 percent (19 260 rpm). Reading 1247.

Figure A2. - Concluded.

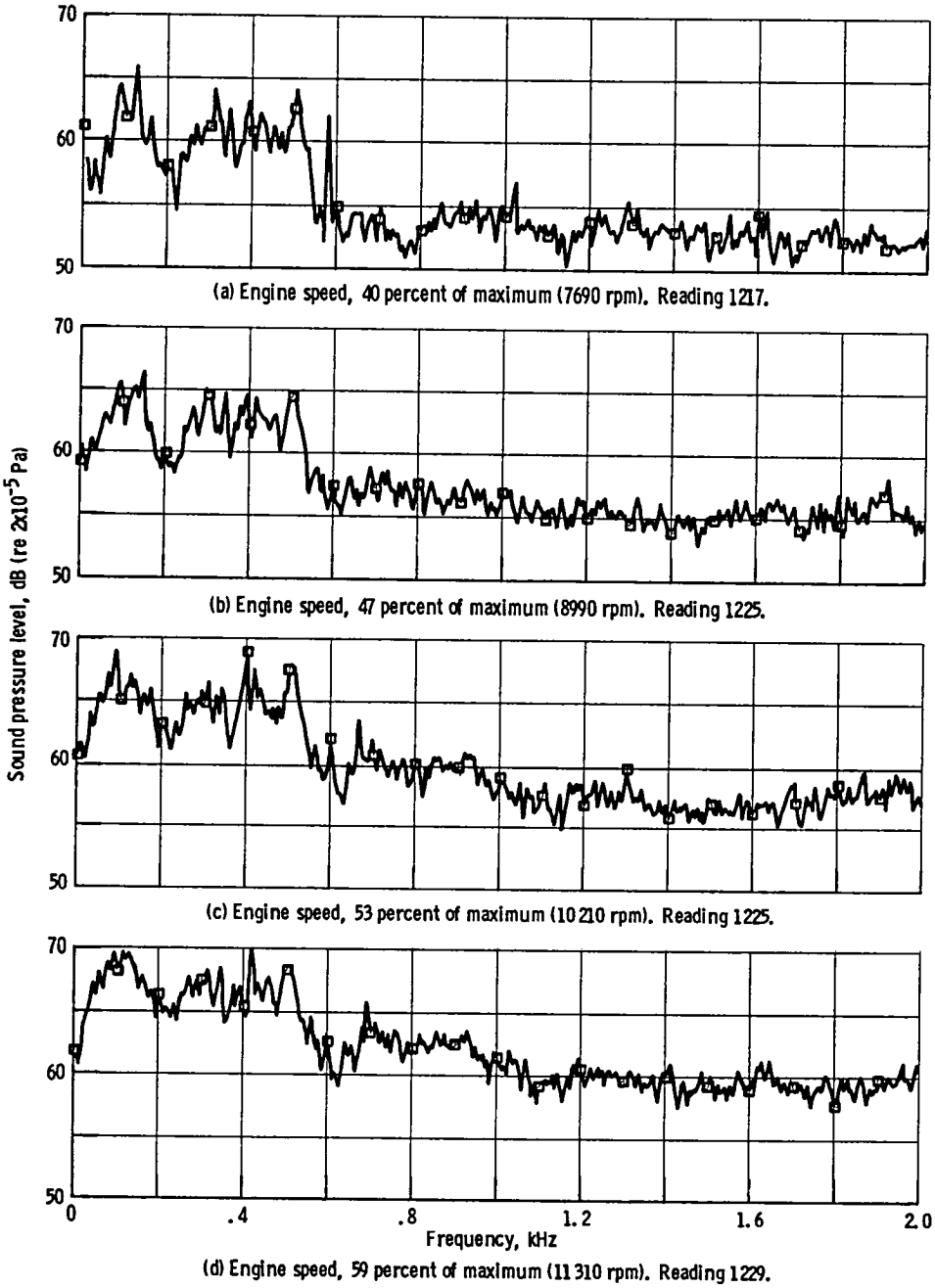

(a) Engine speed, 40 percent of maximum (7690 rpm). Reading 1217.

(b) Engine speed, 47 percent of maximum (8990 rpm). Reading 1225.

(c) Engine speed, 53 percent of maximum (10 210 rpm). Reading 1225.

(d) Engine speed, 59 percent of maximum (11 310 rpm). Reading 1229.

Figure A3. - 120° Far-field sound pressure level with 24.4-m microphone radius for separate-flow nozzle engine configuration. Test AQ4-6; average of 64 samples.

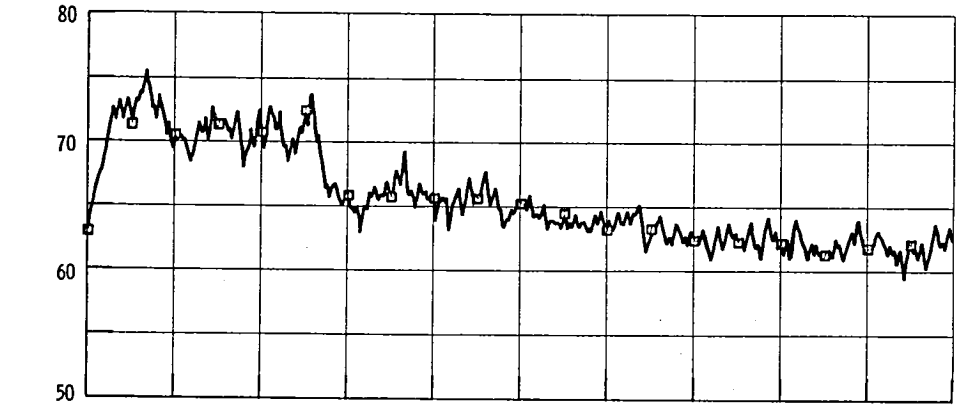

(e) Engine speed, 69 percent of maximum (13 080 rpm). Reading 1233.

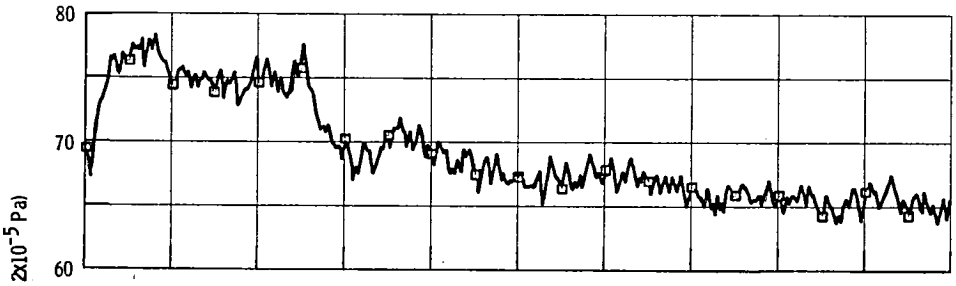

(f) Engine speed, 79 percent of maximum (15170 rpm). Reading 1237.

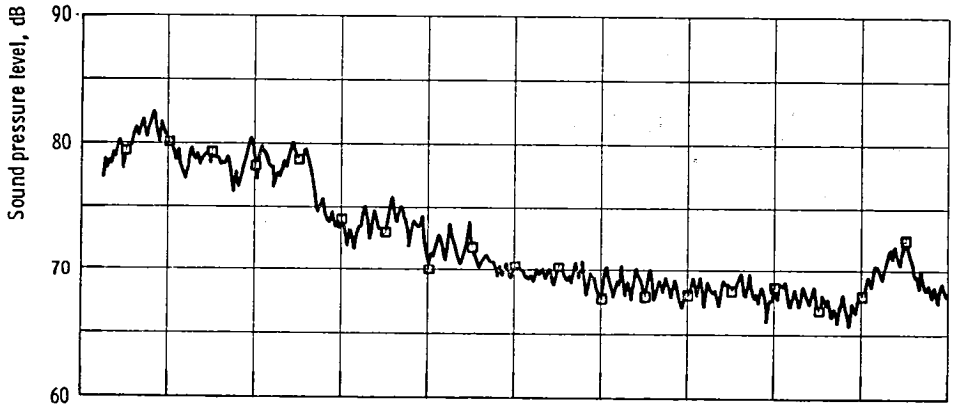

(g) Engine speed, 89 percent of maximum (17160 rpm). Reading 1241.

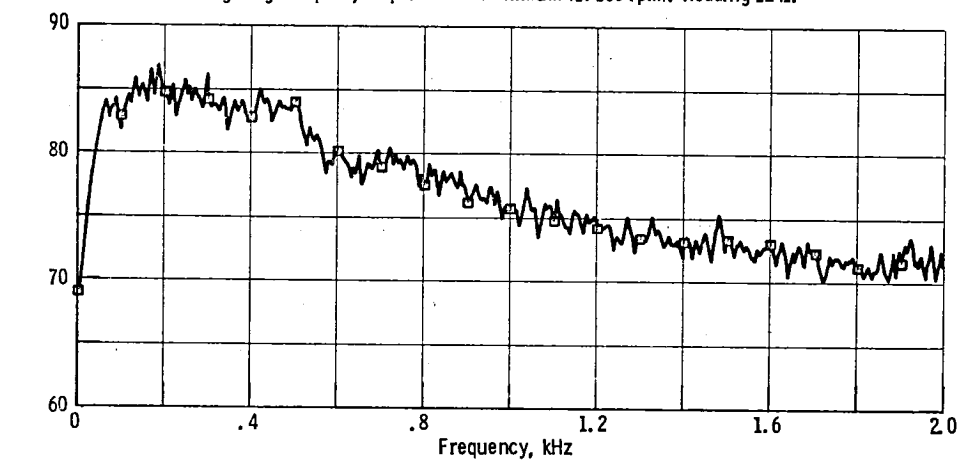

(h) Engine speed, 100 percent (19 260 rpm). Reading 1245.

Figure A3. - Concluded.

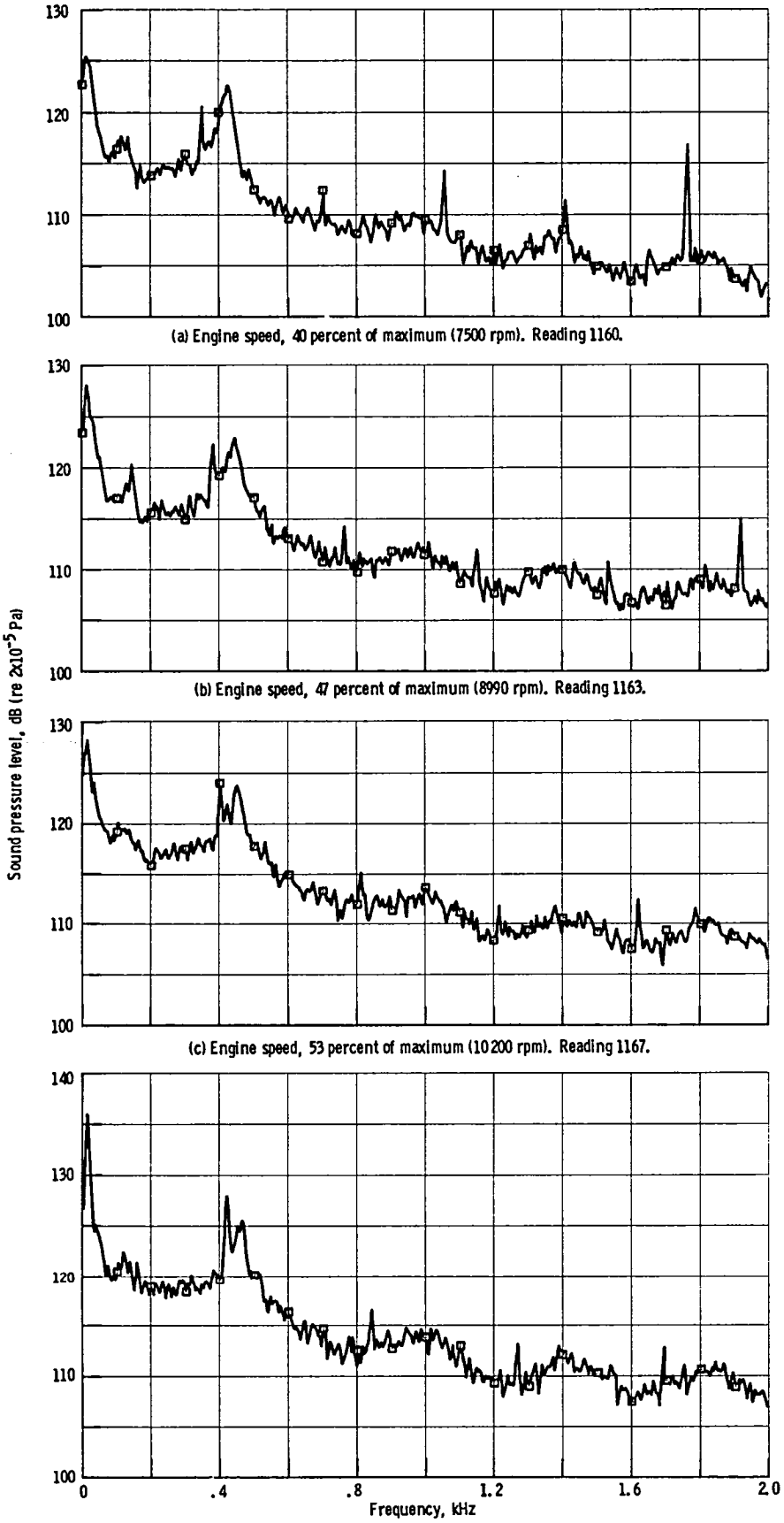

(a) Engine speed, 40 percent of maximum (7500 rpm). Reading 1160.

(b) Engine speed, 47 percent of maximum (8990 rpm). Reading 1163.

(c) Engine speed, 53 percent of maximum (10 200 rpm). Reading 1167.

(d) Engine speed, 59 percent of maximum (11 320 rpm). Reading 1171.

Figure A4. - Combustor pressure spectra for mixer nozzle engine configuration. Test AQ4-1; average of 64 samples.

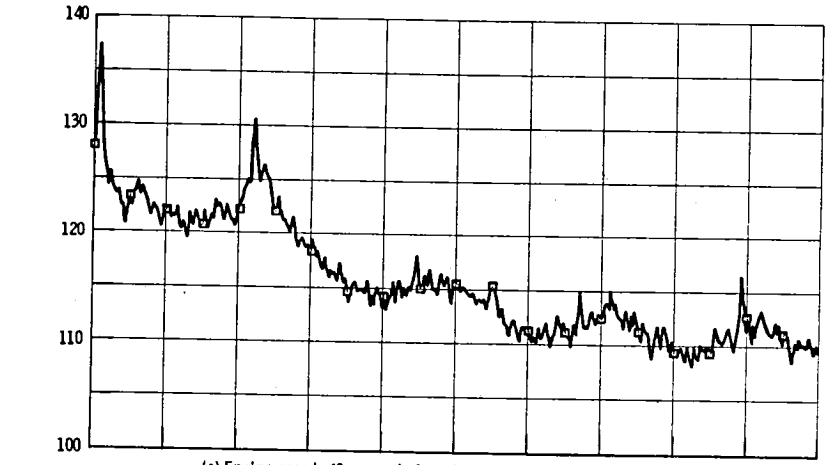

(e) Engine speed, 69 percent of maximum (13 280 rpm). Reading 1175.

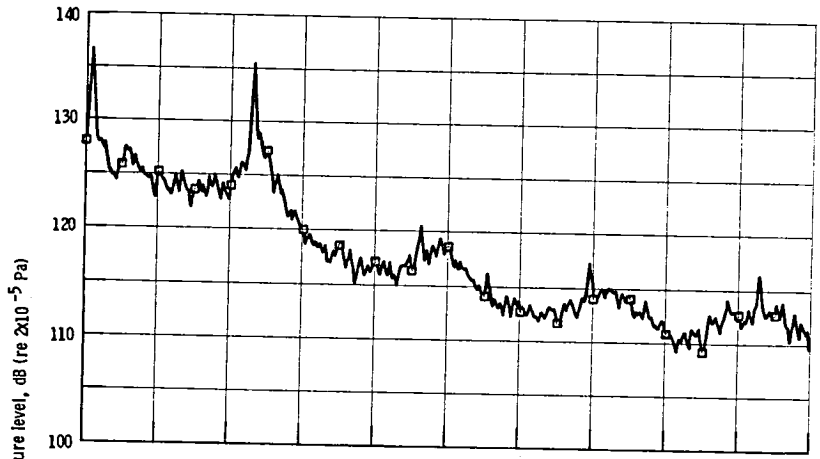

(f) Engine speed, 79 percent of maximum (15190 rpm). Reading 1179.

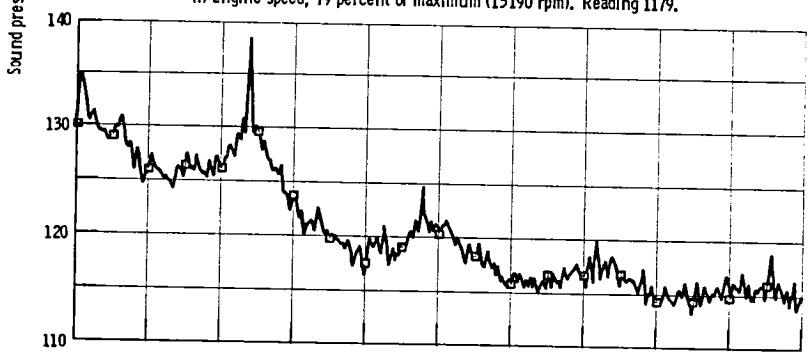

(g) Engine speed, 89 percent of maximum (17 060 rpm). Reading 1183.

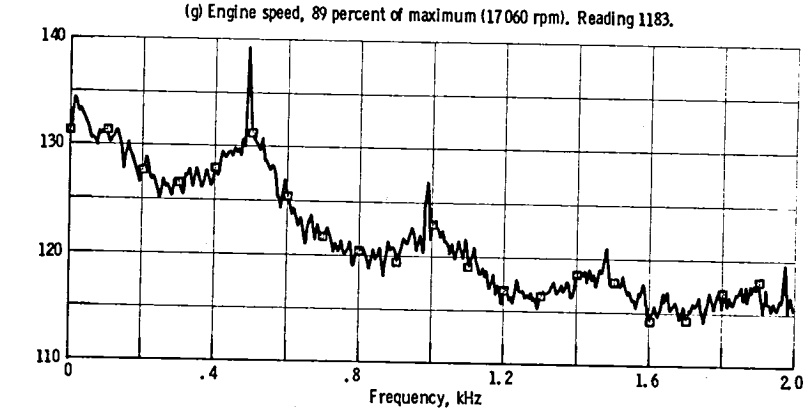

(h) Engine speed, 100 percent (19 080 rpm). Reading 1187.

Figure A4. - Concluded.

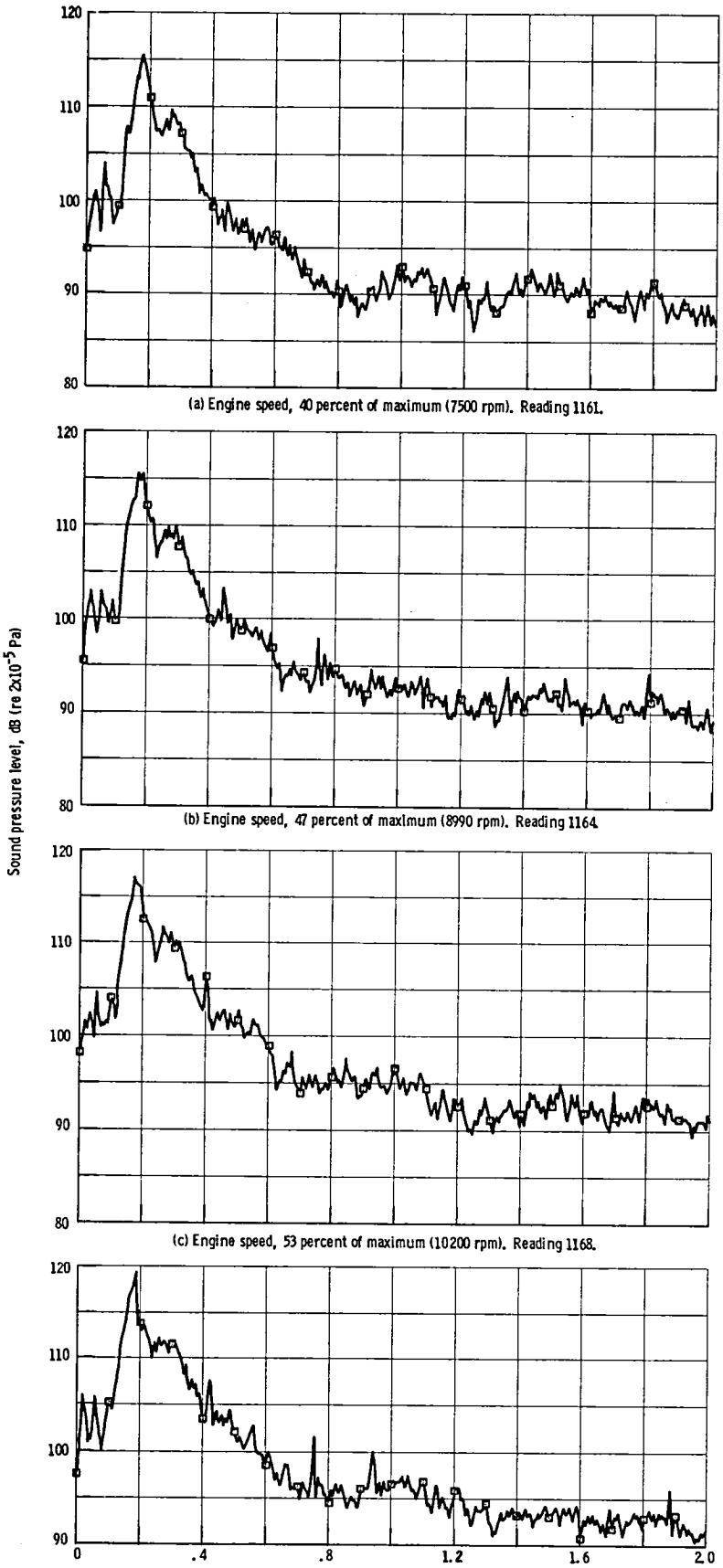

(a) Engine speed, 40 percent of maximum (7500 rpm). Reading 1161.

(b) Engine speed, 47 percent of maximum (8990 rpm). Reading 1164.

(c) Engine speed, 53 percent of maximum (10200 rpm). Reading 1168.

(d) Engine speed, 59 percent of maximum (11320 rpm). Reading 1172.

Figure A5. - Turbine exit pressure spectra for mixer nozzle engine configuration. Test AQ4-1; average of 64 samples.

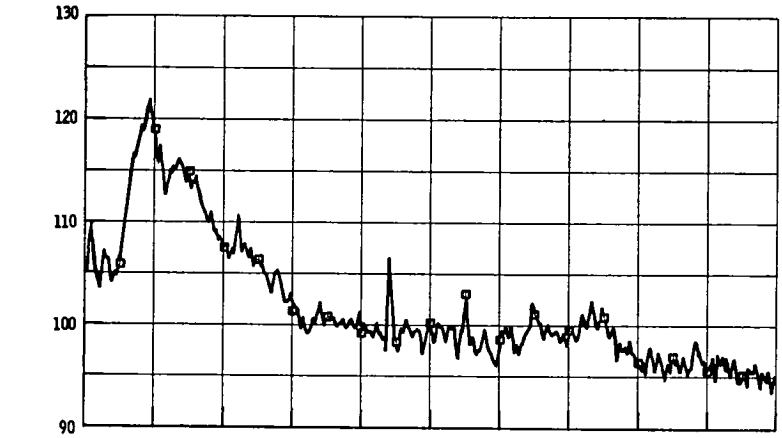

(e) Engine speed, 69 percent of maximum (13 280 rpm). Reading 1176.

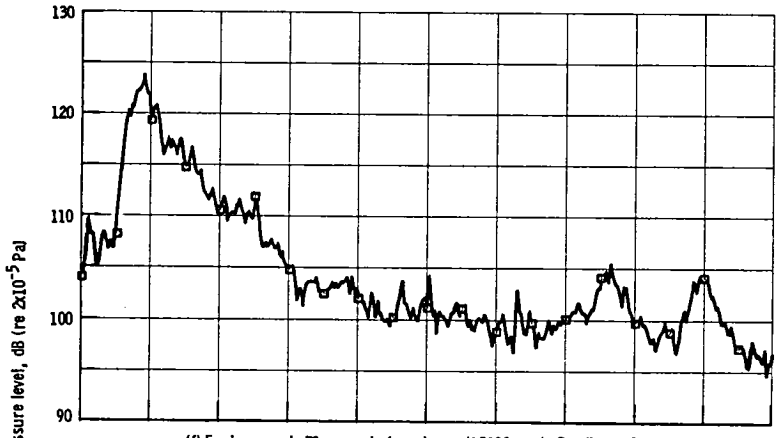

(f) Engine speed, 79 percent of maximum (15 190 rpm). Reading 1180.

Sound pressure level, dB (re 2×10^{-5} Pa)

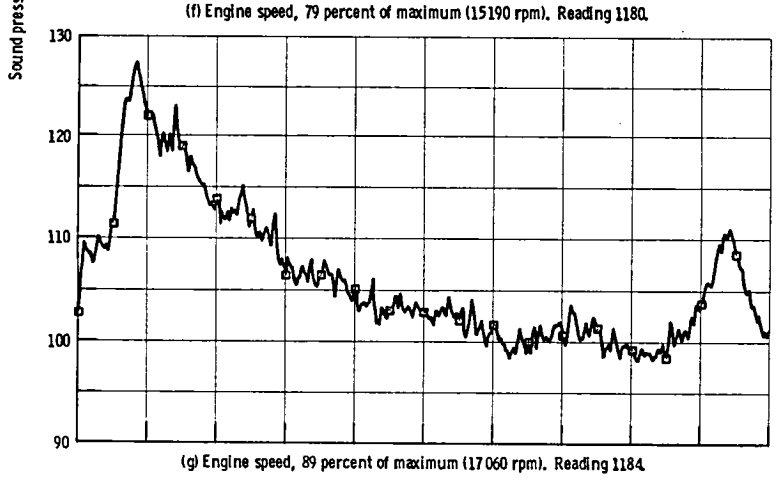

(g) Engine speed, 89 percent of maximum (17 060 rpm). Reading 1184.

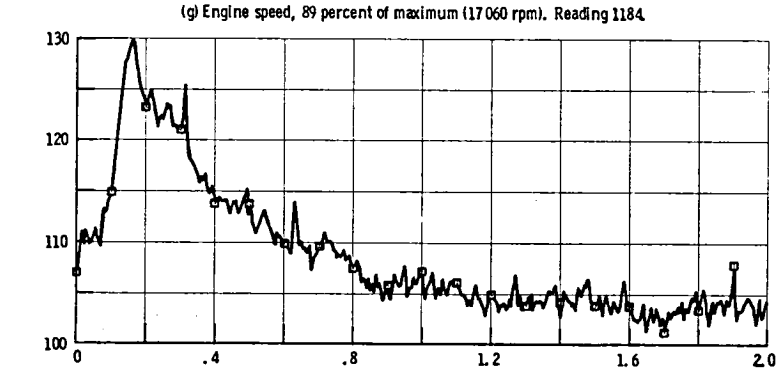

(h) Engine speed, 100 percent speed (19 080 rpm). Reading 1188.

Figure A5. - Concluded.

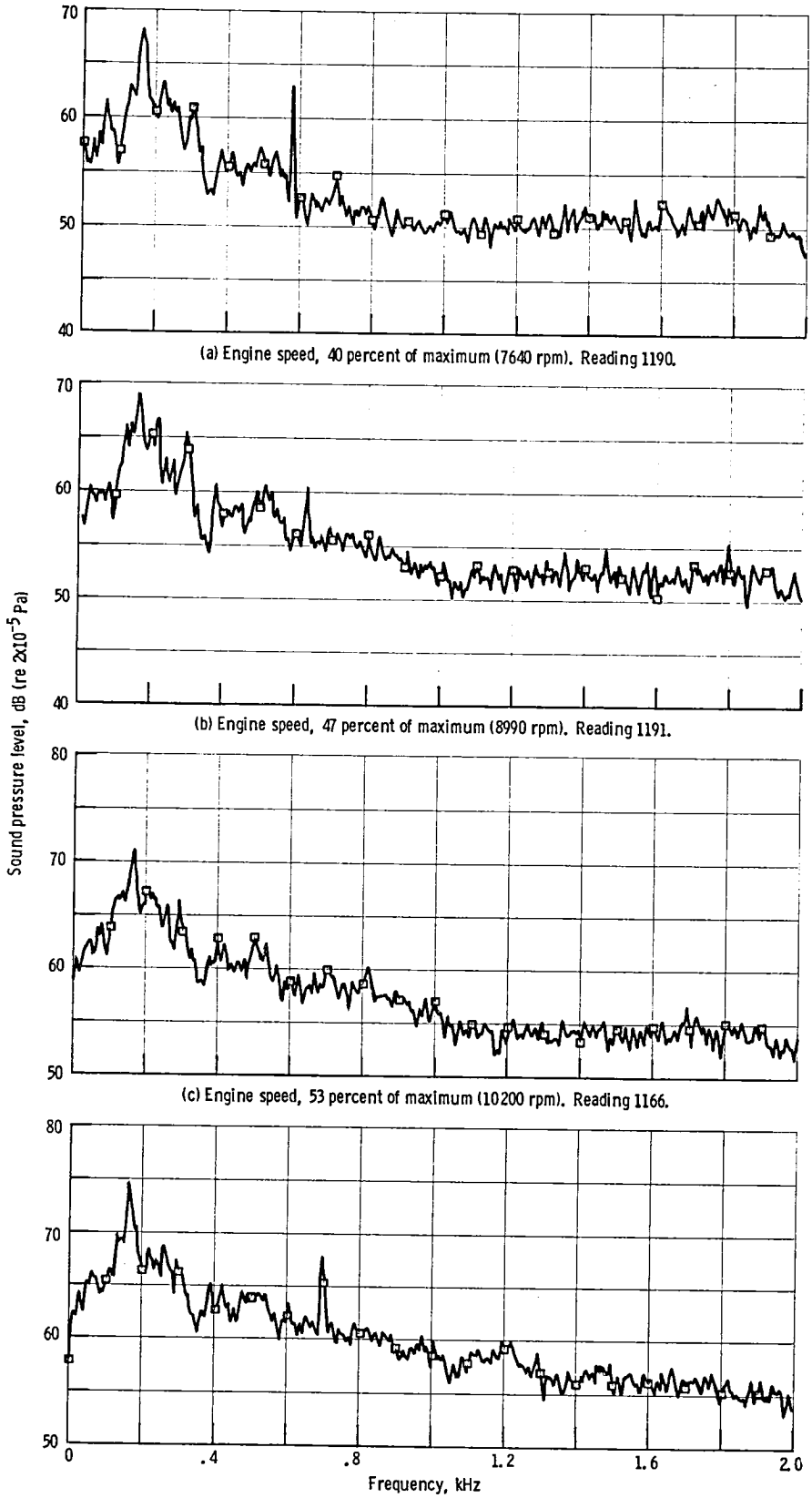

(a) Engine speed, 40 percent of maximum (7640 rpm). Reading 1190.

(b) Engine speed, 47 percent of maximum (8990 rpm). Reading 1191.

(c) Engine speed, 53 percent of maximum (10200 rpm). Reading 1166.

(d) Engine speed, 59 percent of maximum (11320 rpm). Reading 1170.

Figure A6. - 120° Far-field sound pressure level with 24.4-m microphone radius for mixer nozzle engine configuration. Test AQ4-1; average of 64 samples.

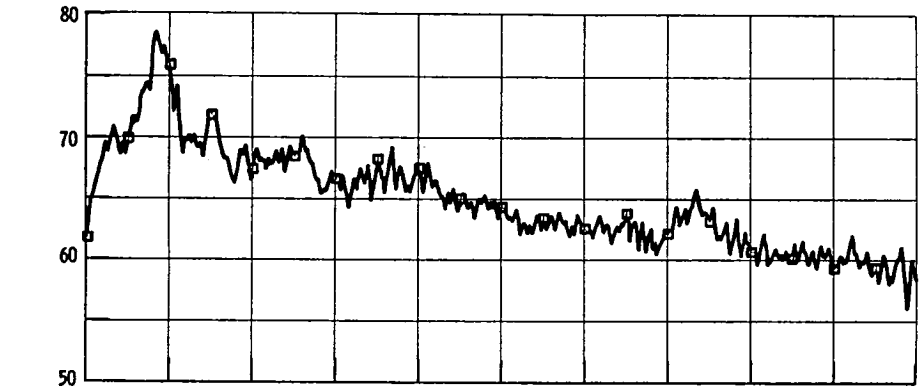

(e) Engine speed, 69 percent of maximum (13 280 rpm). Reading 1174.

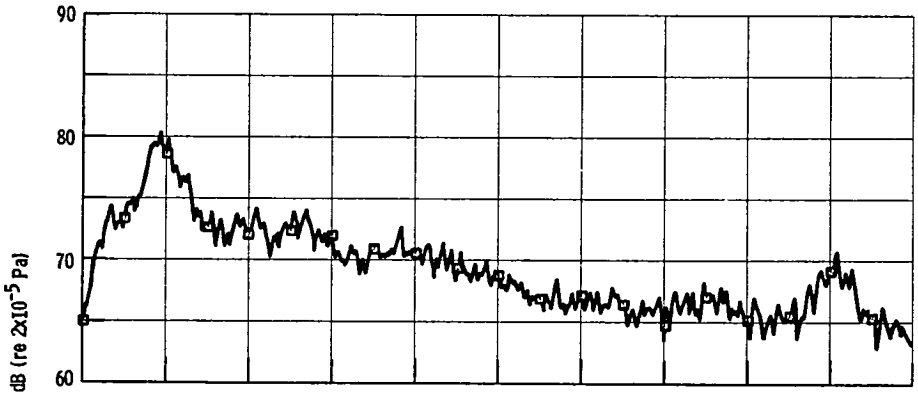

(f) Engine speed, 79 percent of maximum (15190 rpm). Reading 1178.

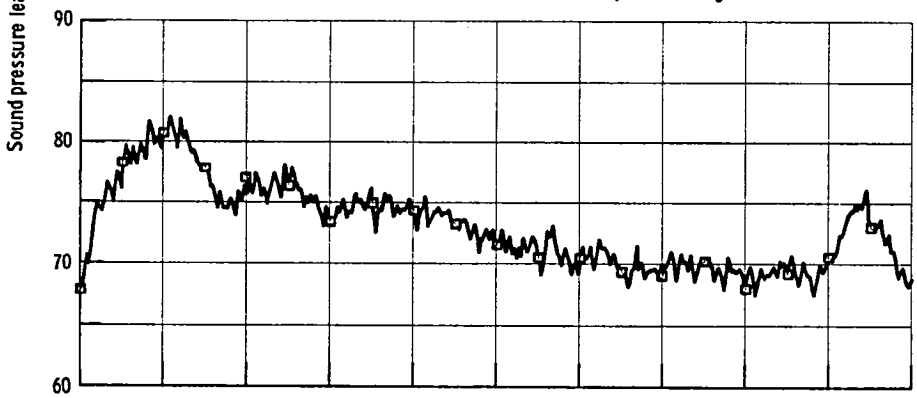

(g) Engine speed, 89 percent of maximum (17 060 rpm). Reading 1182.

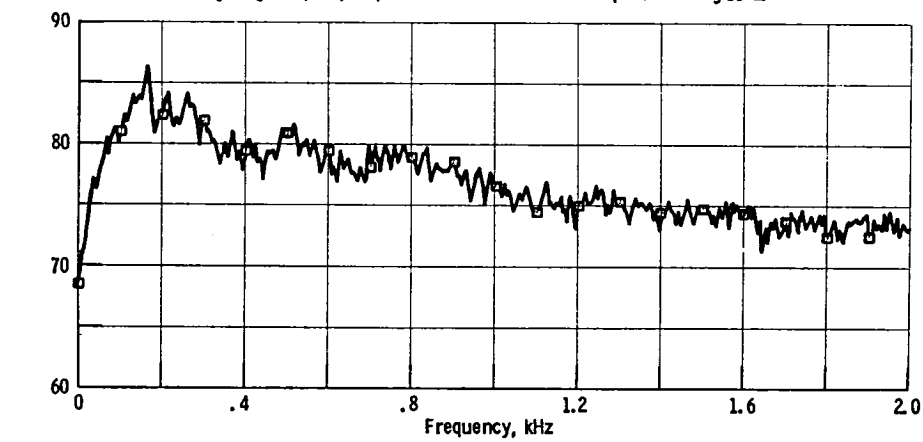

(h) Engine speed, 100 percent of maximum (19 080 rpm). Reading 1186.

Figure A6. - Concluded.

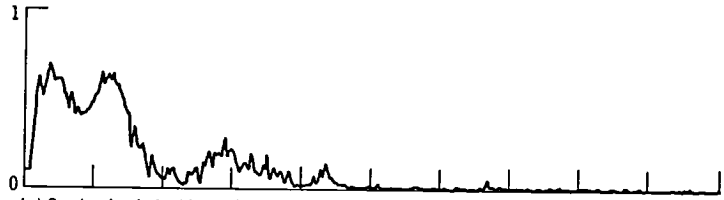

(a) Combustor to turbine exit. Reading 213; number of averages in coherence analysis, N, 6; tape channels 3 and 4.

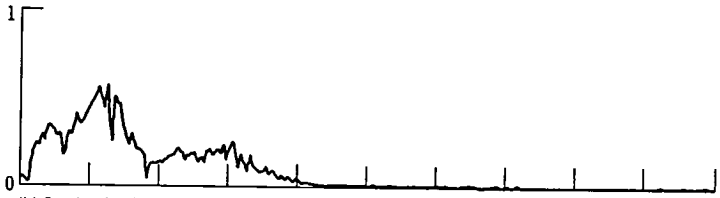

(b) Combustor to nozzle exit. Reading 219; number of averages in coherence analysis, N, 9; tape channels 3 and 13.

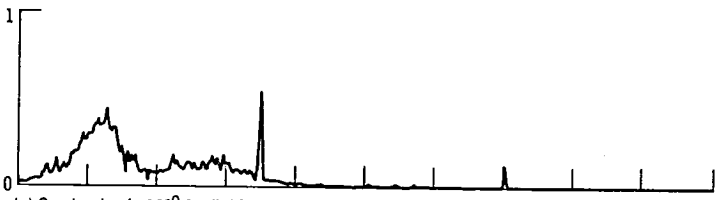

(c) Combustor to 120° far field. Reading 213; number of averages in coherence analysis, N, 9; far-field microphone radius, 24.4 m; tape channels 3 and 10.

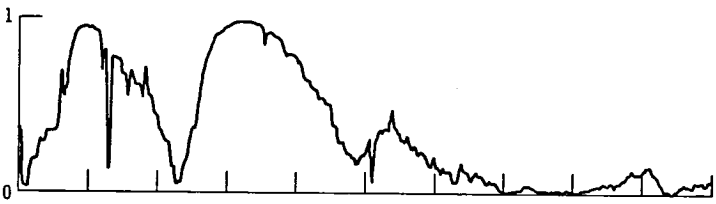

(d) Turbine exit to core nozzle exit. Reading 213; number of averages in coherence analysis, N, 9; tape channels 4 and 13.

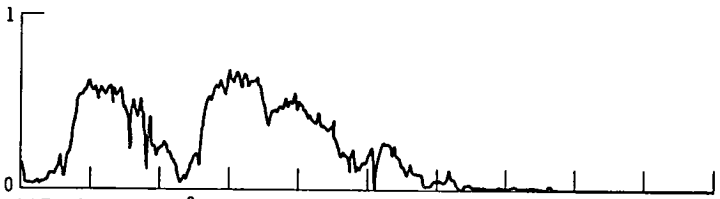

(e) Turbine exit to 120° far field. Reading 213; number of averages in coherence analysis, N, 9; far-field microphone radius, 24.4 m; tape channels 4 and 10.

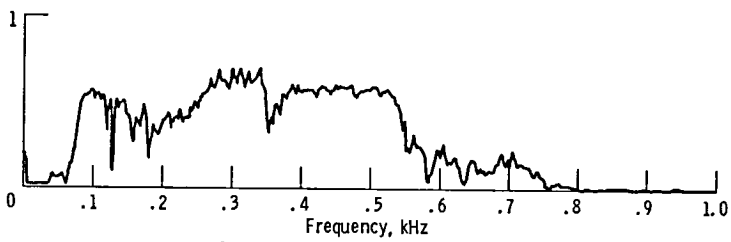

(f) Core nozzle exit to 120° far-field. Reading 213; number of averages in coherence analysis, N, 9; far-field microphone radius, 24.4 m; tape channels 13 and 10.

Coherence function, γ^2

Figure B1. - Coherence functions for separate-flow nozzle engine configuration. Test AQ4-6; engine speed, 40 percent of maximum; bandwidth, 2 Hz.

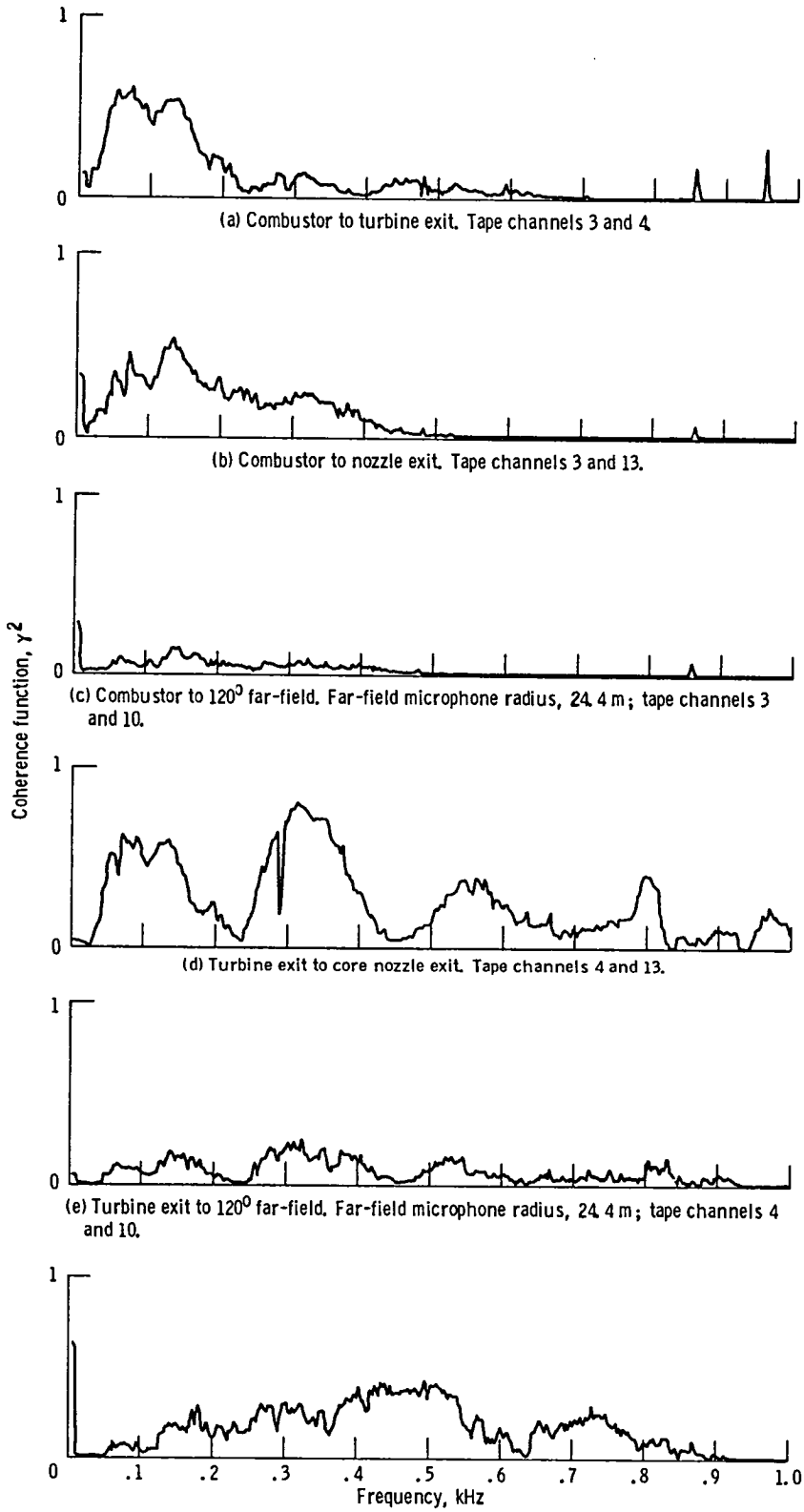

(a) Combustor to turbine exit. Tape channels 3 and 4.

(b) Combustor to nozzle exit. Tape channels 3 and 13.

(c) Combustor to 120° far-field. Far-field microphone radius, 24.4 m; tape channels 3 and 10.

(d) Turbine exit to core nozzle exit. Tape channels 4 and 13.

(e) Turbine exit to 120° far-field. Far-field microphone radius, 24.4 m; tape channels 4 and 10.

(f) Core nozzle exit to 120° far-field. Far-field microphone radius, 24.4 m; tape channels 13 and 10.

Figure B2. - Coherence function for separate-flow nozzle engine configuration. Reading 219; test AQ4-6; engine speed, 89 percent of maximum; bandwidth, 2 Hz; number of averages in coherence analysis, N, 9.

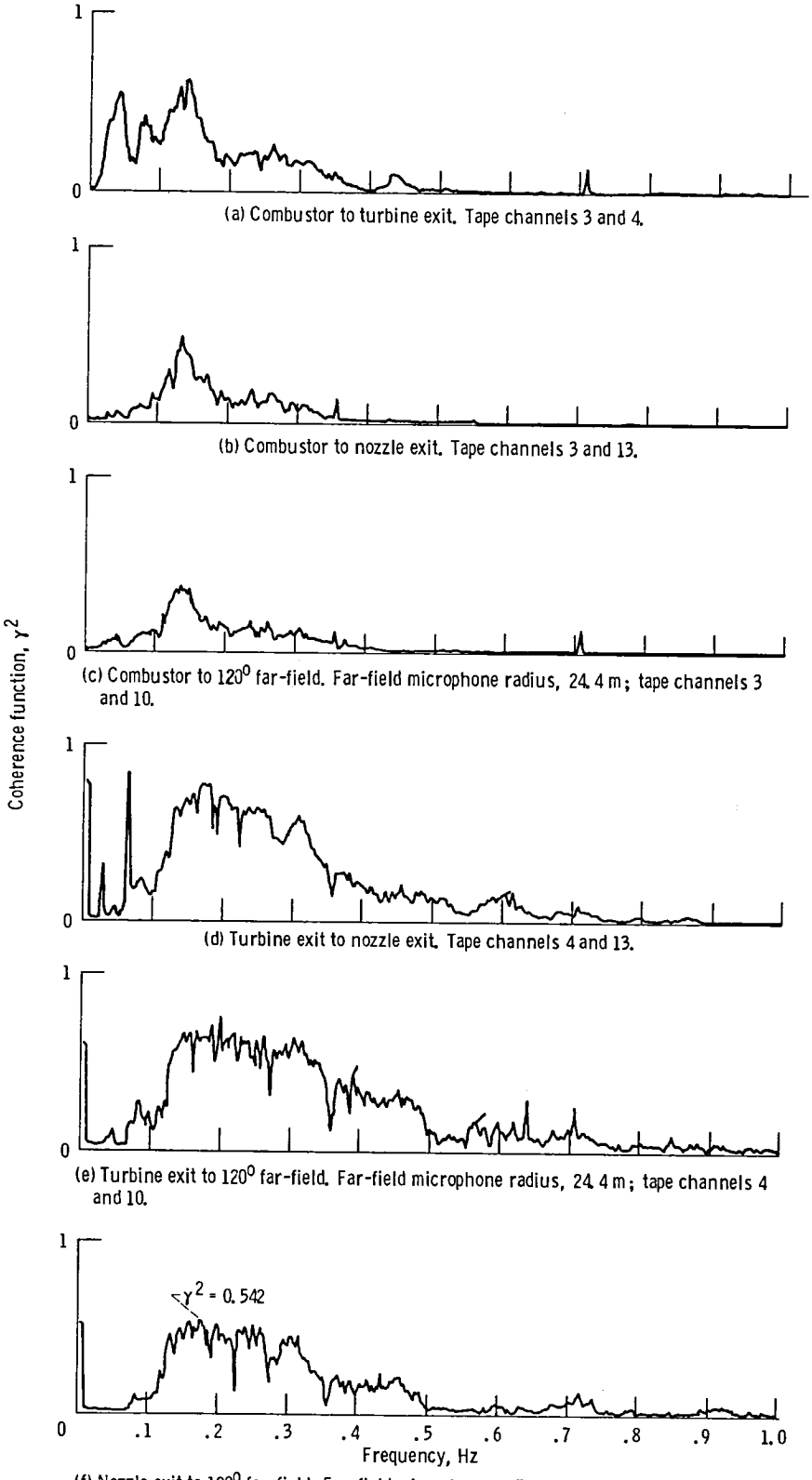

(a) Combustor to turbine exit. Tape channels 3 and 4.

(b) Combustor to nozzle exit. Tape channels 3 and 13.

(c) Combustor to 120° far-field. Far-field microphone radius, 24.4 m; tape channels 3 and 10.

(d) Turbine exit to nozzle exit. Tape channels 4 and 13.

(e) Turbine exit to 120° far-field. Far-field microphone radius, 24.4 m; tape channels 4 and 10.

(f) Nozzle exit to 120° far-field. Far-field microphone radius, 24.4m; tape channels 13 and 10.

Figure B3. - Coherence function for mixer nozzle engine configuration. Reading 145; testAQ4-1; engine speed, 40 percent of maximum; bandwidth, 2 Hz; Number of averages in coherence analysis N, 9.

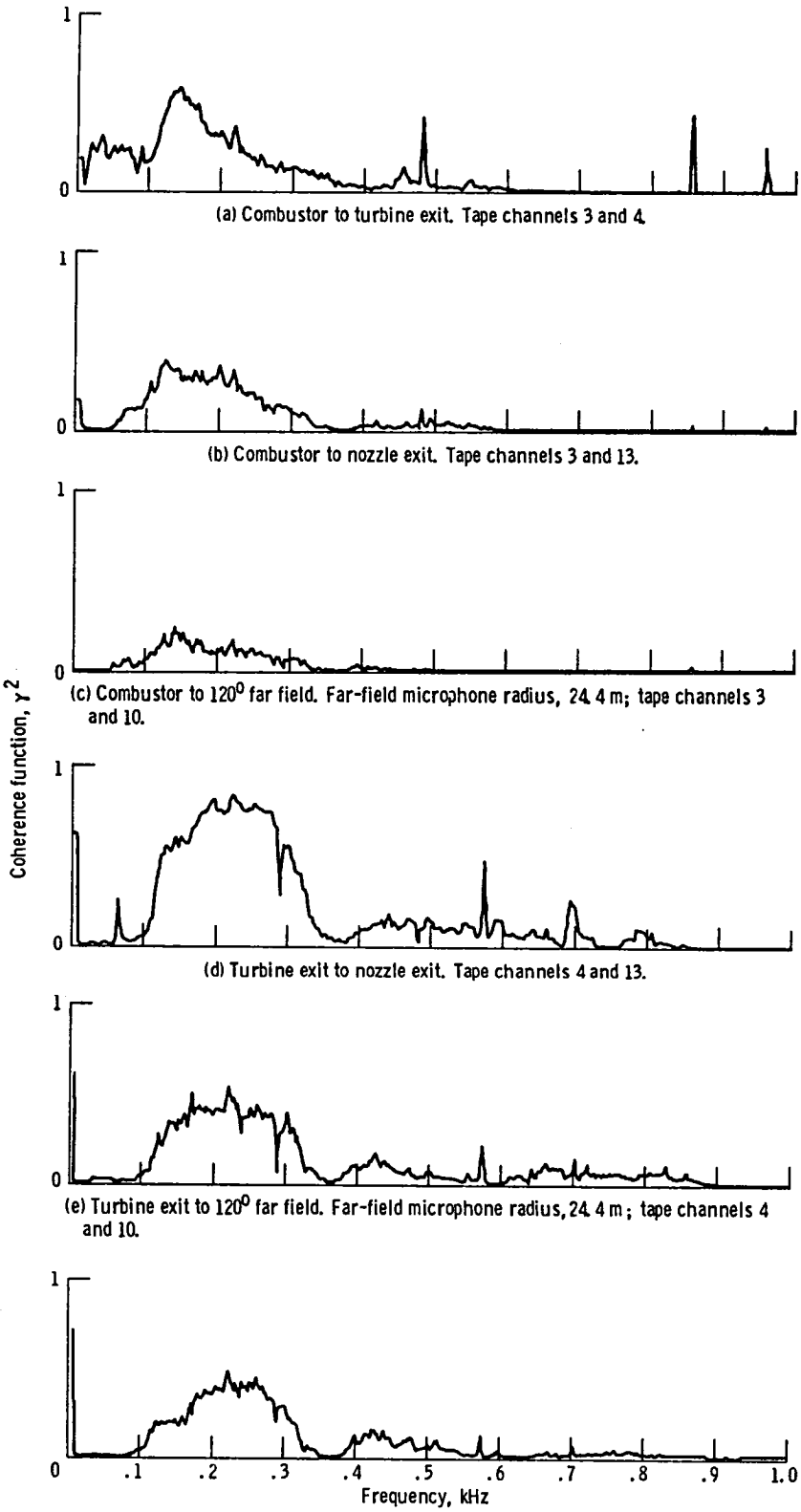

(a) Combustor to turbine exit. Tape channels 3 and 4.

(b) Combustor to nozzle exit. Tape channels 3 and 13.

(c) Combustor to 120° far field. Far-field microphone radius, 24.4 m; tape channels 3 and 10.

(d) Turbine exit to nozzle exit. Tape channels 4 and 13.

(e) Turbine exit to 120° far field. Far-field microphone radius, 24.4 m; tape channels 4 and 10.

(f) Nozzle exit to 120° far field. Far-field microphone radius, 24.4 m; tape channels 13 and 10.

Figure B4. - Coherence function for mixer nozzle engine configuration. Reading 152; test AQ4-1; engine speed, 89 percent of maximum; bandwidth, 2 Hz; number of averages in coherence analysis, N, 9.

1. Report No.	2. Government Accession No.	3. Recipient's Catalog No.
NASA TM-83520		

4. Title and Subtitle	5. Report Date
Low Frequency Noise in a Quiet, Clean, General Aviation Turbofan Engine	January 1984
	6. Performing Organization Code: 505-31-32

7. Author(s)	8. Performing Organization Report No.
Ronald G. Huff, Donald E. Groesbeck, and Jack H. Goodykoontz	E-1879
	10. Work Unit No.

9. Performing Organization Name and Address	11. Contract or Grant No.
National Aeronautics and Space Administration Lewis Research Center Cleveland, Ohio 44135	
	13. Type of Report and Period Covered: Technical Memorandum

12. Sponsoring Agency Name and Address	14. Sponsoring Agency Code
National Aeronautics and Space Administration Washington, D.C. 20546	

15. Supplementary Notes

16. Abstract

A quiet, clean, general aviation, turbofan engine has been instrumented to measure the fluctuating pressures in the combustor, turbine exit duct, engine nozzle and the far field. Both a separate flow nozzle and an internal mixer nozzle were tested. The fluctuating pressure data are presented in overall pressure and power levels and in spectral plots. The combustor data are compared to recent theory and found to be in excellent agreement. The results indicate that microphone correction procedures for elevated mean pressures may be questionable. Ordinary coherence function analysis suggests the presence of an additional low frequency noise source downstream of the turbine that may be due to the turbine itself. Low frequency narrowband data and coherence function analysis are presented.

17. Key Words (Suggested by Author(s))	18. Distribution Statement
Noise; Core engine noise; Combustion noise; Turbine noise; Jet noise; Acoustics; Internal noise	Unclassified - unlimited STAR Category 71

19. Security Classif. (of this report)	20. Security Classif. (of this page)	21. No. of pages	22. Price*
Unclassified	Unclassified		

*For sale by the National Technical Information Service, Springfield, Virginia 22161

National Aeronautics and
Space Administration

Washington, D.C.
20546

Official Business
Penalty for Private Use, $300

SPECIAL FOURTH CLASS MAIL
BOOK

Postage and Fees Paid
National Aeronautics and
Space Administration
NASA-451

NASA

POSTMASTER: If Undeliverable (Section 158
Postal Manual) Do Not Return